Chapter-2

To investigate changes in TRIM34-sensitive ubiquitination pathway genes in lung cancer cell lines.

Chapter 2: To investigate changes in TRIM34-sensitive ubiquitination pathway genes in lung cancer cell lines.

INTRODUCTION

Lung cancer remains a significant global health challenge, accounting for a considerable number of cancer-related deaths[26,275]. Despite progress in detection and treatment, the overall survival rate for lung cancer patients remains low due to its complex and heterogeneous nature[223]. In recent years, recombination DNA technologies have revolutionized cancer research, with the Clustered Regularly Interspaced Short Palindromic Repeats (CRISPR) and associated proteins (Cas) system, commonly referred to as CRISPR/Cas9 emerging as a potent gene editing tool[276–283]. The pursuit of a dependable and efficient gene-editing tool within viable cells has long been a goal for biomedical researchers. Once the CRISPR mechanism in prokaryotes was comprehended, scientists recognized its potential utility in humans, plants, and other microorganisms[284]. Originally identified as a bacterial immune response against viral infections, this system has been harnessed and adapted for precise DNA manipulation across diverse organisms, including eukaryotic cells[285]. The convergence of molecular biology, bioinformatics, and biotechnology has culminated in the development of a versatile and programmable platform that enables targeted genetic modifications with unprecedented efficiency and accuracy. This technology allows precise genomic modifications, enabling researchers to investigate gene functions in cancer cells[286]. The CRISPR/Cas9 system has transformed the landscape of genetic engineering by enabling precise modifications to genomes across diverse organisms. At the core of this technology lies the Cas9 endonuclease, guided by guide RNAs (gRNAs), to introduce targeted DNA cleavage. Understanding the intricate molecular interactions and mechanisms underlying the CRISPR/Cas9 system is crucial for harnessing its potential in scientific research, therapeutic applications, and biotechnology[287–291].

The ubiquitin-proteasome system is a crucial mechanism responsible for the degradation of intracellular proteins, marking them for destruction through ubiquitination. This dynamic process is important for maintaining cellular homeostasis by eliminating misfolded or damaged proteins and regulating key cellular functions [97,118,292]. Metabolic reprogramming, a hallmark of cancer, involves complex changes in biosynthesis and energy metabolism. Recent studies highlight the role of ubiquitination, a crucial post-translational modification, in regulating cancer metabolism[293]. Dysregulation of the UPS has been implicated in various diseases, including cancer, where aberrant protein degradation can contribute to tumorigenesis[293,294]. E3 ubiquitin ligases, influential enzymes in ubiquitination, play a key role in cancer by regulating tumor-promoting or suppressing pathways. Their specificity and involvement in cancer hallmarks have led to the development of compounds targeting E3 ligases for cancer therapy[123]. Maintaining a dynamic balance between ubiquitination and deubiquitination is crucial for health.

In lung cancer, disruptions in these processes affecting tumor suppressors or carcinogens, contribute to disease progression. UPS emerges as a promising avenue for lung cancer drug development, particularly targeting proteasomes and E3s. Precise ubiquitination and degradation of oncogene proteins, facilitated by technologies like PROTAC, hold potential for innovative lung cancer therapeutics[295]. The TRIM family of proteins acting as E3 ubiquitin ligases, characterized by the presence of a conserved tripartite motif, has emerged as a critical player in this intricate system, participating in diverse cellular functions[182,212,231,232]. The intricate nature of TRIM proteins, with their diverse functions in immune response regulation, signal transduction pathways, and cellular homeostasis, underscores their significance as potential modulators of carcinogenesis [55,154]. TRIM proteins influence the degradation of key signaling components (e.g., p53, NF-κB, PI3K/AKT) through ubiquitin-dependent proteolysis[128]. In NSCLC cells, it was observed that TRIM can affect several signaling pathways to have an anti-tumor activity[296,297]. The TRIM34, alternatively known as IFP1 and RNF21, belongs to the tripartite motif (TRIM) family and is situated on chromosome 11p15. The TRIM family members are frequently involved in various cellular processes such as innate immunity, autophagy, intracellular signaling, and carcinogenesis. Additionally, they possess E3 ubiquitin ligase activity[154,298]. Wang Y. *et al.* (2015) have identified the regulatory functions of TRIMs in multiple signaling pathways mediated by interferon response and inflammation[160]. Previous studies have revealed that it has an important antiviral role in blocking HIV-1 replication via targeting viral capsid[299]. Research shows that *TRIM34* expression is upregulated in response to Type I IFNs[270]. Moreover, Lian *et al.* (2021) have found that novel role that TRIM34 has a protective role against colon cancer[218]. The TRIM34 protein localizes to the mitochondria and can induce apoptosis by releasing cytochrome C, disrupting mitochondrial membrane potential (MMP) [270]. Wang *et al.* (2022) have shown that TRIM34 interacts with ZBP1, a sensor for influenza A virus (IAV), promoting K63-linked polyubiquitination. This interaction triggers IAV-induced cell death and inflammation, protecting mice from IAV-related death. TRIM34's role in ZBP1 polyubiquitination establishes TRIM34 as a key regulator in IAV-induced programmed cell death[300].

In Chapter 1, it was noted that our observations imply a plausible correlation between IFN-γ stimulation and the induction of cancer regression via TRIM34-mediated apoptosis. The next logical step is to investigate the impact on cancer cell characteristics in the absence of TRIM34. Therefore, a knockout study was conducted. This study aims to provide insights into the alterations occurring in post-translational modifications, such as ubiquitylation, shedding light on the processes involved in cancer progression. Our objective is to unravel the complex role of TRIM34 within the context of lung cancer. Through comprehensive molecular analyses, including transcriptomic profiling we aim to elucidate the specific changes induced by TRIM34 knockout in lung adenocarcinoma cells.

Additionally, functional assays will shed light on the consequences of TRIM34 knockout on essential cellular behaviors.

MATERIAL AND METHODS

Cell lines: NCI-H23 cells were used for the study. The cell maintenance process is provided in the Material and methods section.

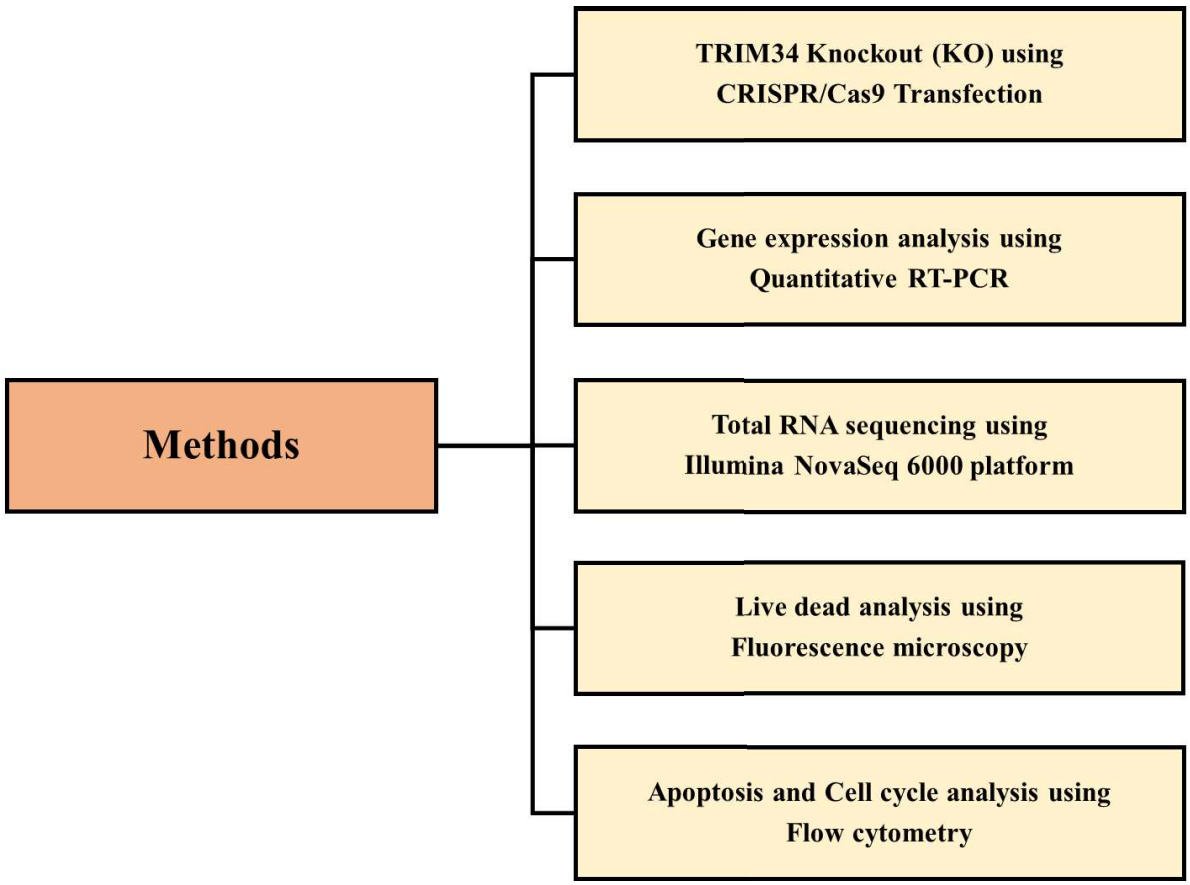

Figure 2.1: Illustration of the experimental procedure utilized in the present investigation.

Detailed methodology is described in the material and methods section.

Transfection of CRISPR/Cas9 and total RNA Sequencing methodology as follows:

Transfection study by CRISPR/Cas9

Cells were seeded at a density of 1.5 x 10^5 cells per well with 3 ml of antibiotic-free standard growth medium 24 hours prior to transfection. The cell confluency was maintained at 40% for successful transfection. Cells were transfected with TRIM34 CRISPR/Cas9 KO Plasmid (h) (Santa Cruz Biotechnology, cat. no. sc-417920) and Negative Control plasmid (Santa Cruz Biotechnology, cat. no. sc-418922), each in their respective wells. This transfection process was carried out using the UltraCruz Transfection Reagent (Santa Cruz Biotechnology, cat. no. sc-395739) according to the manufacturer's instructions. Cells were incubated with Plasmid DNA and transfection reagent complex for 48 hours, and successful transfection was visually confirmed through green fluorescent protein (GFP).

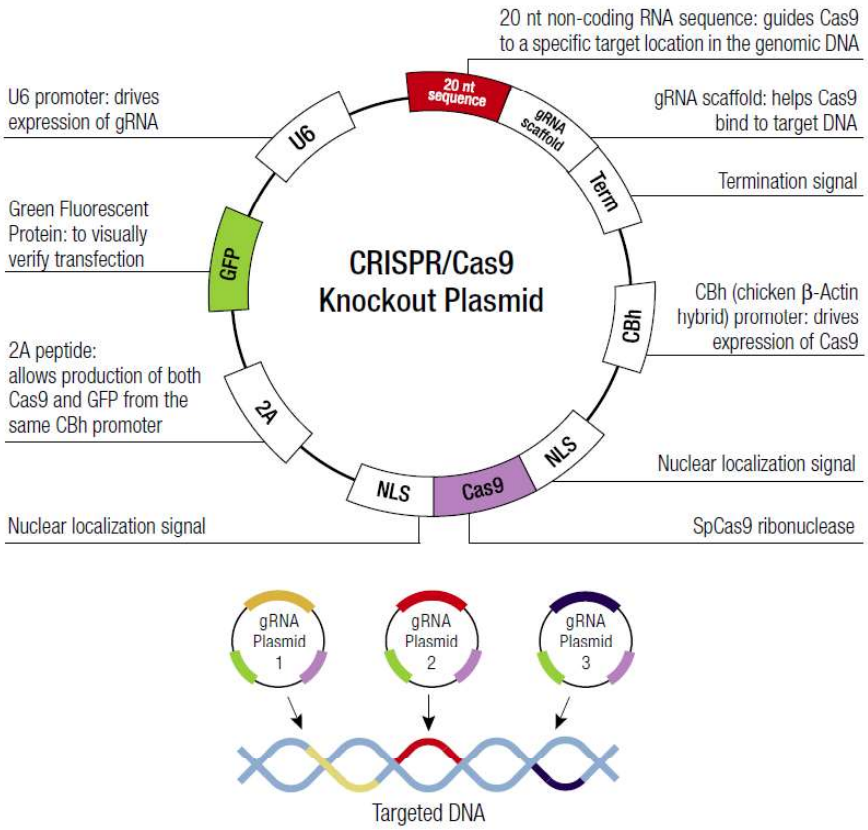

Figure 2.2: TRIM34 CRISPR/Cas9 KO Plasmid

Total RNA Sequencing:

- **RNA Isolation and Purification**

Transfected cells were collected in 1 ml of TRIzol, and a micromotor pestle was used for cell dissociation. Following that, 200 µl of chloroform was added, and the mixture was vigorously shaken for 15 seconds. It was then incubated at room temperature for 3 minutes, followed by another round of shaking and centrifugation at 12,000 g for 15 minutes at 4°C. The colorless layer was carefully transferred to a new tube, and an equal volume of 75% ethanol was added and incubated at room temperature for 2 minutes. The sample was then loaded onto a PureLink RNA Mini kit column and post centrifugation, the flow-through was discarded. After a washing process, 80 µl of working Purelink DNase was added. After 15 minutes incubation, wash buffer 1 was added again, and centrifugation was performed. This step was repeated, with the second centrifugation lasting for 2 minutes and 30 seconds. The column lid was opened, allowing the column to dry. Then, 35 µl of

RNAse-free water was added to the column membrane, followed by incubation at room temperature for 1 minute. The column was centrifuged at 12,000 g for 1 minute and RNA was stored at -80°C until further processing.

Table 6: Prepared working PureLink DNase.

Component	Volume/Sample
10X DNase I Reaction Buffer	8 µl
Resuspended DNase (~3U/µl)	10 µl
RNase Free Water	62 µl
Final Volume	80 µl

- **Analysing RNA Yield and Quality**

The quality control (QC) assessment of RNA was executed through a series of molecular assays. Initially, RNA quantification was carried out using the Qubit™ RNA quantification kit (cat. no. Q10211). Subsequently, for a comprehensive evaluation of RNA quality, high sensitivity electrophoresis was employed. High Sensitivity electrophoresis is a valuable technique for assessing the integrity and size distribution of RNA fragments within the sample. To further enhance the precision of the QC analysis, this assessment was conducted using the Agilent 2200 TapeStation system. The in-built software allowed for the determination of the RNA integrity number (RIN), automatically assigning an integrity value to the total RNA sample. The RIN value provides an objective metric of total RNA quality, with a range from 10 (indicating highly intact RNA) to 1 (indicating completely degraded RNA).

- **Library Preparation for Total RNA Sequencing for The Illumina Platforms.**

The oligo hybridization and rRNA depletion protocol were executed to prepare RNA samples for sequencing by eliminating ribosomal RNA (rRNA) and other non-targeted RNA molecules, thereby enriching the specific RNA population of interest. Initially, 1 µg of total RNA was dissolved in 10 µl of RNase-free water to facilitate further processing.

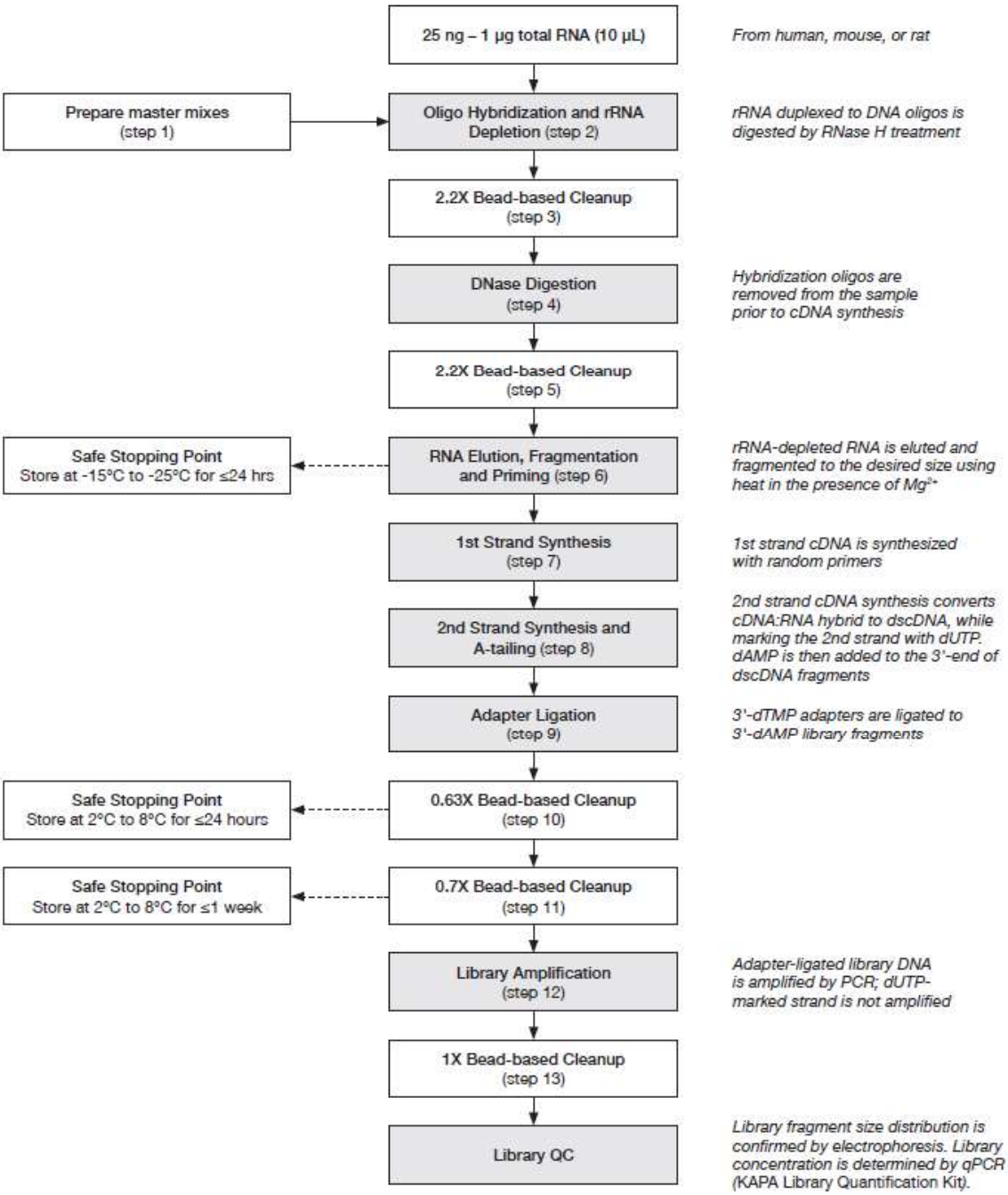

Figure 2.3: Workflow of library preparation for total RNA sequencing for the illumina platforms.

- **Oligo Hybridization and rRNA Depletion**

The rRNA hybridization reactions were initiated by mixing 10 µl of total RNA in water with 10 µl of the hybridization master mix at room temperature.

Table 7: Hybridization master mix.

Component	1 library
Hybridization Buffer	4 µl
Hybridization Oligos (HMR)	4 µl
RNase-free water	2 µl
Total master mix volume:	10 µl

Table 8: Hybridization using the following thermocycling conditions.

Step	Temp.	Duration
Hybridization	95°C	2 min
Ramp down to 45°C at -0.1°C/s		
Pause	45°C	∞
Add depletion master mix		
Depletion	45°C	30 min
Hold	4°C	∞

Subsequently, the prepared reaction mixture was introduced into the thermocycler equipped hybridization. In depletion, temperature was maintained at 45°C for a duration of 30 minutes. At this temperature, 5 µl of the depletion master mix containing RNase H was added to each hybridization reaction (20 µl) and thoroughly mixed by pipetting.

Table 9: Depletion master mix

Component	1 library
Depletion Buffer	3 µl
RNase H	2 µl
Total master mix volume:	5 µl

- **rRNA depletion cleanup**

To perform the rRNA depletion cleanup, a bead-based cleanup was carried out by combining 25 µl of the rRNA-depleted RNA with 55 µl of pure beads, resulting in a total volume of 80 µl. The beads were thoroughly resuspended by vortexing at 1600 rpm for 2 minutes. The plate containing the reaction mixtures was then incubated at room temperature for 5 minutes to facilitate the binding of RNA to the beads. Subsequently, a magnet was used to capture the beads, and the supernatant containing unwanted RNA molecules was carefully removed and discarded. For the washing step, the beads were incubated on a magnet at room temperature for 30 seconds with 200 µl of 80% ethanol twice to eliminate any remaining impurities. The ethanol was carefully removed and discarded, without disturbing the beads. Finally, the beads were allowed to air-dry at room temperature for 3 – 5 minutes, ensuring complete evaporation of all ethanol.

- **DNase Digestion**

Table 10: DNase digestion master mix

Component	Per library
DNase Buffer	2.2 µl
DNase	2 µl
RNase-free water	17.8 µl
Total master mix volume:	22 µl

After the rRNA depletion cleanup, the RNA samples were subjected to DNase digestion to remove hybridization oligonucleotides from the ribosomal-depleted RNA. To assemble the DNase digestion reactions, 22 µl of the rRNA-depleted RNA was mixed with 22 µl of the DNase digestion master mix at room temperature. The reaction mixture was vortexed at 1600 rpm for 1 minute and incubated at room temperature for 3 minutes to elute the RNA off the beads. The liquid was then cleared by using a magnet to capture the beads. Next, 20 µl of the supernatant was carefully transferred into a new plate. The DNase digestion reaction was carried out at 37°C for 30 minutes using a thermocycler, followed by an immediate proceeding to the DNase digestion cleanup.

- **DNase Digestion Cleanup**

The DNase digestion cleanup was performed using a bead-based cleanup. Initially, 20 µl of the DNase-treated RNA was mixed with 44 µl pure beads. The beads were thoroughly resuspended by pipetting, and the plate containing the reaction mixtures were incubated at room temperature for 5 minutes to allow the RNA to bind to the beads. The supernatant containing unwanted RNA molecules was carefully removed and discarded, and the beads were washed with 200 µl of 80% ethanol twice. Following the washes, the beads were dried at room temperature for 3 – 5 minutes to completely remove all ethanol.

- **RNA Elution, Fragmentation, and Priming**

The beads containing purified, DNase-treated RNA were thoroughly resuspended in 22 µl of 'Fragment, Prime, and Elute Buffer' (1X) by pipetting. They were then vortexed at 1600 rpm for 30 seconds. The tubes containing the reaction mixtures were incubated at room temperature for 3 minutes and then centrifuged at 300 rpm to elute the RNA from the beads. A magnet was used to capture the beads, clearing the liquid. Subsequently, 20 µl of the supernatant was carefully transferred into new tubes, with the tubes containing the beads being discarded. The fragmentation and priming program were executed in a thermocycler at a temperature of 94°C for 6 minutes. This step ensured the appropriate fragmentation of RNA and the addition of primers for subsequent strand synthesis. The tubes were placed on ice, and the process proceeded immediately to 1st strand synthesis.

- **1st strand synthesis**

Table 11: 1st strand synthesis master mix:

Component	Per library
1st strand synthesis buffer	11 µl
KAPA Script	1 µl
Total master mix volume:	12 µl

The 1st strand synthesis reaction was assembled using 20 µl of fragmented, primed RNA and 10 µl of 1st strand synthesis master mix. The reaction mixture was mixed and incubated at specific temperatures for primer extension, 1st strand synthesis, and enzyme inactivation.

Table 12: 1st strand synthesis using the following thermocycling conditions.

Step	Temp.	Duration
Primer extension	25°C	10 min
1st strand synthesis	42°C	15 min
Enzyme inactivation	70°C	15 min
Hold	4°C	∞

- **2nd strand synthesis and A-tailing**

Table 13: 2nd strand synthesis and A-tailing master mix

Component	Per library
2nd strand marking buffer	31 µl
2nd strand synthesis & A-Tailing Enzyme Mix	2 µl
Total master mix volume:	33 µl

The 2nd strand synthesis and A-tailing were executed to convert the cDNA into a double-stranded DNA library. The 2nd strand synthesis and A-tailing reaction were assembled using 30 µl of the 1st strand synthesis product and 30 µl of the 2nd strand synthesis and A-tailing master mix. The reaction mixture was mixed thoroughly by vortexing at 1600 rpm for 30 sec and incubated at specific temperatures for 2nd strand synthesis and A-tailing.

Table 14: 2nd strand synthesis and A-tailing using the following thermocycling profile.

Step	Temp.	Duration
2nd strand synthesis	16°C	30 min
A-tailing	62°C	10 min
Hold	4°C	∞

- **Adapter Ligation**

Table 15: Adapter ligation master mix

Component	Per library
Ligation Buffer	40 µl
DNA Ligase	10 µl
Total master mix volume:	50 µl

Specific adapters were ligated to the double-stranded DNA library. The reaction was initiated by combining 60 µl of the A-Tailed dscDNA with 45 µl of the adapter ligation master mix and 5 µl of the 1.5 µM adapter. The resulting reaction mixture was meticulously mixed through repeated pipetting. Subsequently, the mixture was subjected to vortexing at 1600 rpm for 30 seconds, followed by a brief spin-down, after which it was incubated at 20°C for a duration of 15 minutes.

- **1st Post-ligation Cleanup**

Following the adapter ligation, the 1st post-ligation cleanup was performed to eliminate unligated adapters and other contaminants. 110 µl of the adapter-ligated DNA was mixed with 70 µl of beads and vortexed at 1600 rpm for 30 seconds, followed by an incubation period of 5-15 minutes to facilitate DNA binding to the beads. The plate was then placed on a magnet to capture the beads. Carefully, 175 µl of supernatant was removed and discarded. The remaining beads were washed twice with 200 µl of 80% ethanol at room temperature, each time allowing for a 30-second incubation. The ethanol was then carefully removed and discarded. The beads were air-dried and resuspended in 50 µl of 10 mM Tris-HCl (pH 8.0 – 8.5). The plate was incubated at room temperature for 2 minutes to elute DNA from the beads.

- **2nd Post-ligation Cleanup**

The 2nd post-ligation cleanup is performed to further purify the adapter-ligated DNA. In this step, 50 µl of the beads with purified, adapter-ligated DNA were mixed with 35 µl of PEG/NaCl solution, resulting in a total volume of 85 µl. The beads were thoroughly resuspended and subjected to vortexing at 1600 rpm for 30 seconds, followed by an incubation period lasting between 5 to 15 minutes to facilitate the binding of DNA to the beads. The plate was then placed on a magnet to capture the beads and incubated until the liquid became clear. Subsequently, 80 µl of supernatant was carefully removed and discarded. The beads were then subjected to two rounds of washing with 200 µl of 80% ethanol at room temperature, with each time allowing for a 30-second incubation, and the ethanol was carefully removed and discarded. The beads were allowed to dry at room temperature. Following the drying step, the beads were resuspended in 22 µl of 10 mM Tris-HCl (pH 8.0 – 8.5). The plate was incubated

at room temperature for 2 minutes to elute the DNA from the beads. Plate was then placed on a magnet to capture the beads and incubated until the liquid turned clear. Subsequently, 20 µl of the clear supernatant was transferred to a new tube in preparation for library amplification.

Library Amplification

Table 16: Library amplification master mix

Component	1 library
KAPA HiFi HotStart ReadyMix (2X)	25 µl
Library Amplification Primer Mix (10X)	5 µl
Total master mix volume:	30 µl

The described protocol was executed as follows: 20 µl of purified, adapter-ligated DNA was combined with 30 µl of the library amplification master mix in each library amplification reaction. Adequate mixing was achieved by pipetting.

Table 17: Amplified the library using the following thermocycling profile

Step	Temp.	Duration	Cycles
Initial denaturation	98°C	45 sec	1
Denaturation	98°C	15 sec	8
Annealing	60°C	30 sec	
Extension	72°C	30 sec	
Final extension	72°C	1 min	1
Hold	4°C	∞	1

- **Library Amplification Cleanup**

The purification of the amplified libraries was carried out according to the following protocol. 50 µl of the amplified library DNA was combined with an equal volume of beads, resulting in a final volume of 100 µl. The beads were thoroughly resuspended by vortexing at 1800 rpm for 2 minutes. Subsequently, the mixture was incubated for 10 minutes and subjected to two washes with 200 µl of 80% ethanol. The beads were left to air-dry at room temperature until complete evaporation of all residual ethanol. Once dried, the beads were resuspended in 22 µl of 10 mM Tris-HCl buffer (pH 8.0 – 8.5). After 2 minutes incubation, plate was placed on a magnet to capture the beads, and incubation was continued until the liquid turned clear. 20 µl of the supernatant, which now contained the purified and amplified libraries, was carefully transferred to a new tube and stored at -80°C until further analysis.

- **NGS Libraries' quality control (QC) assessment**

The purified, amplified libraries can now be quantified to determine their concentration and ensure that they meet the desired sequencing output. The quality control (QC) assessment of the Next-Generation Sequencing (NGS) library was performed using a combination of molecular assays. Initially, the quantification of double-stranded DNA (dsDNA) within the library was conducted utilizing Invitrogen™ Qubit™ dsDNA quantification assay kit (cat. no. Q32854). Subsequently, for a comprehensive evaluation of library quality, high sensitivity DNA electrophoresis was employed. This analysis was carried out using the Agilent 2200 TapeStation System, which provides high-resolution visualization and quantification of DNA fragments, thus ensuring the rigorous quality control of the NGS library. Following quantification, the libraries were employed for Total RNA sequencing on an Illumina NovaSeq 6000 platform at National Institute of Biomedical Genomics, Kolkata, India, generating ~50 million reads per sample.

- **The RNA Seq analysis**

It starts with the initial quality assessment and adapter trimming of the raw Fastq files. These processed Fastq files are then aligned to a reference genome obtained from NCBI using the DRAGEN RNA aligner. Following alignment, Transcripts Per Million (TPM) files are generated for each sample. The raw count matrix is derived from the quantification files using the txtimport tool. Since there are no replicates, count normalization is performed using edgeR, and differential analysis is conducted to compare the control and test groups. Log2 Fold change values are calculated to identify genes with differential expression. Significantly expressed genes are selected based on a log2 fold change threshold of +/- 1.5 and an adjusted *p*-value less than 0.05.

Protein-Protein Interaction Network and hub gene prediction

A collection of significantly altered Differentially Expressed Genes (DEGs), was subjected to the STRING (Search Tool for the Retrieval of Interacting Genes/Proteins) version 12 database, an online resource accessible at https://string-db.org/. This database facilitates the exploration of diverse interconnections among the designated targets, forming an intricate web of protein-protein interactions. The resulting interactions.tsv file from STRING was imported into Cytoscape software, version 3.10, which serves as a sophisticated platform for network visualization and analysis[301]. Within the Cytoscape environment, the intricate biological Protein-Protein Interaction (PPI) network was scrutinized utilizing a suite of Cytoscape plugins, notably the CytoHubba toolkit. Employing this toolkit, a comprehensive assessment of the complex PPI network was conducted. Employing the CytoHubba plugin facilitated this in-depth analysis, enabling the discernment of the ten most

prominent hub nodes[302]. These hub nodes were ranked based on their degree centrality scores within the Protein-Protein Interaction (PPI) network.

Assessment of gene enrichment

Gene enrichment is a systematic analytical approach applied to collections of genes, employing the gene ontology categorization system to classify genes into predefined clusters based on their functional characteristics. The classification system presented is organized around three primary domains within the Gene Ontology: biological activities, cellular activities, and molecular activities. The concept of "biological activities" encompasses the fundamental cellular or metabolic significance inherent in genes' participation within the complex web of genetic interactions. This entails the coordinated cooperation of genes to fulfill overarching biological functions. "Cellular activities" delve into the diverse roles executed by gene products within the intricate microenvironment of the cell, contributing significantly to the cell's overall functionality and playing vital roles in various biological processes. Simultaneously, "molecular activities" emphasize the specific molecular functions undertaken by individual genes, ranging from enzymatic activities to receptor binding and other molecular interactions.

An additional valuable resource in this context is the Kyoto Encyclopedia of Genes and Genomes (KEGG), a comprehensive database that provides insights into biological systems. Utilizing KEGG pathway analysis enables to unveil intricate connections and interdependencies among crucial genes. This analytical approach facilitates a more profound understanding of the fundamental biological processes regulated by these genes. In our investigation, Differentially Expressed Genes (DEGs) were subjected to analysis using the SRplot[303]. This web-based platform offered a means to visually represent and further scrutinize the characteristics and patterns of these DEGs, aiding in gaining deeper insights into their potential functional roles and regulatory implications.

RESULTS

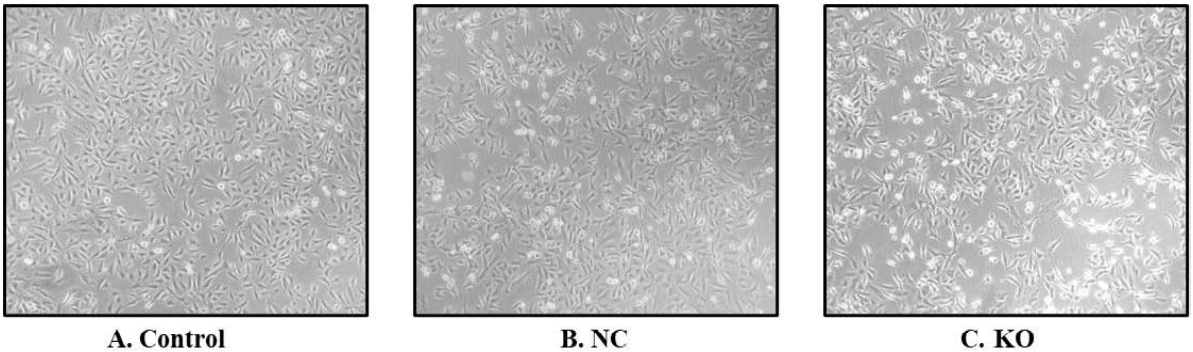

Figure 2.4: Morphological changes of the cells in **A**. Control, **B**. transfection of Negative Control plasmid, and **C.** transfection of TRIM34 CRISPR/Cas9 plasmid.

In the control group (Fig. 2.4A), untreated cells exhibited a normal morphology, characteristic of NCI-H23 cells. In the negative control group (Fig. 2.4B), no guide RNA (gRNA) was introduced, to ensure no off-target effects are resulted by transfection and plasmid itself. The negative control cells exhibited cellular morphology typical of NCI-H23 cells. The absence of any specific genetic manipulation or targeting maintained the normal appearance and behavior of the cells. On the other hand, in the *TRIM34* knockout cells (Fig. 2.4C), where the CRISPR-Cas9 system specifically targeted and disrupted the *TRIM34* gene, we observed distinct morphological changes. These knockout cells showed an altered morphology, many cells lost their ability to adhere, indicating disrupted cellular integrity.

The morphological analysis in the knockout group underscores the specificity of the observed changes, directly associated with the knockout of the TRIM34 gene. This experiment further supports the notion that the observed morphological alterations are a consequence of the targeted TRIM34 gene knockout and not due to any non-specific effects of the transfection process.

Verification of *TRIM34* knockdown at the transcript level in NCI-H23 lung adenocarcinoma cells.

We employed the CRISPR-Cas9 gene-editing technique to target and knockout the *TRIM34* gene in NCI-H23 cells. The objective was to investigate the specific role of *TRIM34* in the cellular context of these lung cancer cells. We designed three experimental groups to examine the impact of *TRIM34* gene knockout in NCI-H23 cells. The first group served as the control, where cells were not subjected to any genetic manipulation. The second group consisted of cells transfected with Negative Control (NC), ensuring that any observed effects were specific to the *TRIM34* knockout and not due to the transfection process itself. Lastly, the third group involved the actual *TRIM34* knockout (KO), achieved through CRISPR-Cas9 gene editing. After performing the gene knockout, we confirmed its success through quantitative real-time polymerase chain reaction (qRT-PCR), a sensitive method to measure gene expression levels. The qRT-PCR analysis revealed a significant reduction in the transcript levels of *TRIM34* compared to the control group ($p \leq 0.01$) and negative control ($p \leq 0.001$), indicating that the targeted gene was effectively silenced. This reduction in *TRIM34* expression provides evidence that the CRISPR-Cas9 approach successfully disrupted the gene's function in NCI-H23 cells.

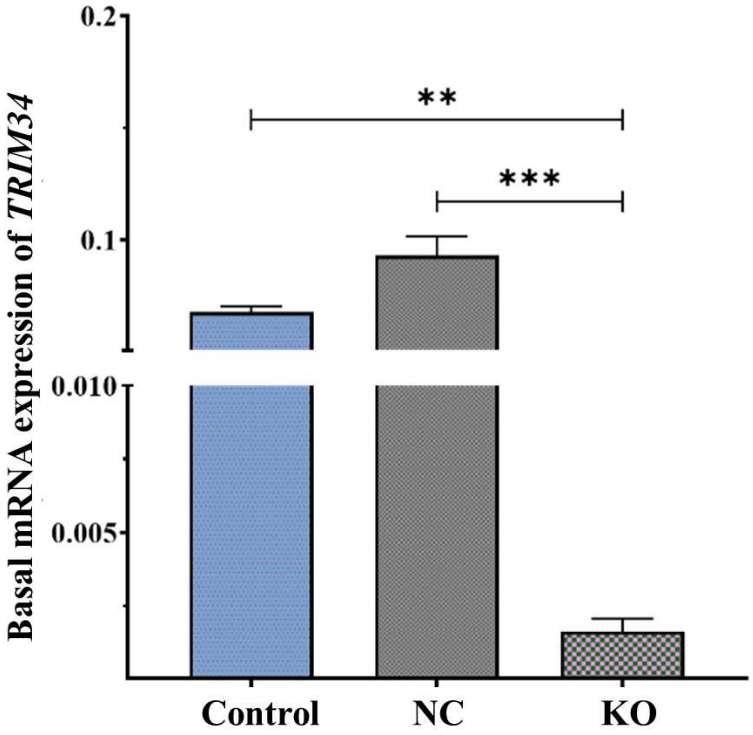

Figure 2.5: Transcript level confirmation of *TRIM34* knockdown in lung adenocarcinoma NCI-H23 cells. mRNA expression of *TRIM34* was measured by real-time qRT-PCR and normalized to *GAPDH* gene expression. Graphs are plotted as Mean ± SEM. (n=3). Statistical significance is denoted by **, and ***, to indicate $p \leq 0.01$, and $p \leq 0.001$, respectively.

Evaluation of cell viability in NCI-H23 after transfection.

We sought to investigate the impact of *TRIM34* gene knockout on cell viability in NCI-H23 cells. To assess cytotoxicity and cell viability, we employed the Cytotoxicity kit, utilizing Calcein AM and Ethidium homodimer-1 (EthD-1) staining. Following the transfection and staining process, we used fluorescence microscopy to visualize and quantify the percentage of cell death in each group. The results demonstrated that the Control group exhibited a minimal percentage of cell death at 0.18%. In the Negative control group, the percentage of cell death increased slightly to 0.6%, but this difference did not reach statistical significance compared to the Control group. However, in the *TRIM34* CRISPR/Cas9 KO Transfection group, a significant elevation ($p \leq 0.01$) in cell death was observed, with a percentage of 2.55%. These findings indicate that the knockout of the *TRIM34* gene contributed to a notable increase in cell death in NCI-H23 cells. The data suggests that *TRIM34* may play a role in cell survival, and its disruption through CRISPR/Cas9 gene editing resulted in decreased cell viability.

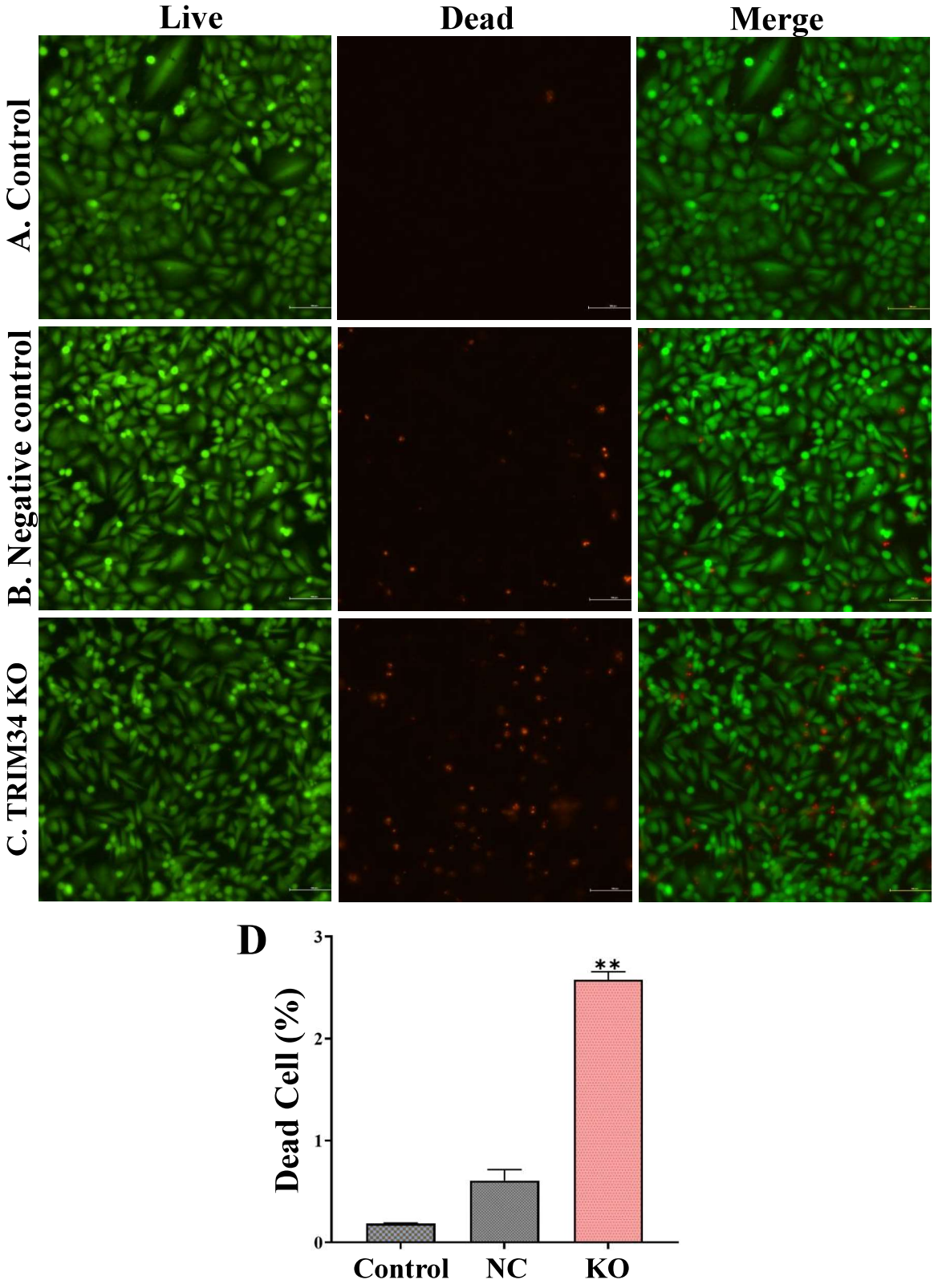

Figure 2.6: Assessment of cell viability using Calcein AM and Ethidium Homodimer-1 (EthD-1) staining in NCI-H23. Calcein AM stains for live cells in green, and EthD-1 stains for dead cells in red. **A**. Control (Untreated) Cells, **B**. Negative Control Group: Cells transfected with CRISPR/Cas9 lacking Guide RNA **C.** *TRIM34* CRISPR/Cas9 KO Transfected cells. **D.** Measurement of the proportion of dead cells in each group using ImageJ software. ** stands for $p \leq 0.01$ to indicate statistical significance. Scale bar: 100 μm.

Apoptosis analysis using FACS.

After transfection, we investigated the effect of *TRIM34* gene knockout on apoptosis in NCI-H23 cells using Annexin V-FITC and propidium iodide (PI) staining. After FACS analysis, the Apoptosis index (%) was determined, revealing 3.05% for both the Control and Negative Control groups (A&B), while the *TRIM34* CRISPR/Cas9 KO transfection group (C) exhibited a significantly increased ($p \leq 0.01$) Apoptosis index of 6.3%. These results indicate that the knockout of the *TRIM34* gene induced a substantial rise in apoptotic cell death in NCI-H23 cells, suggesting a potential role for *TRIM34* in regulating apoptosis.

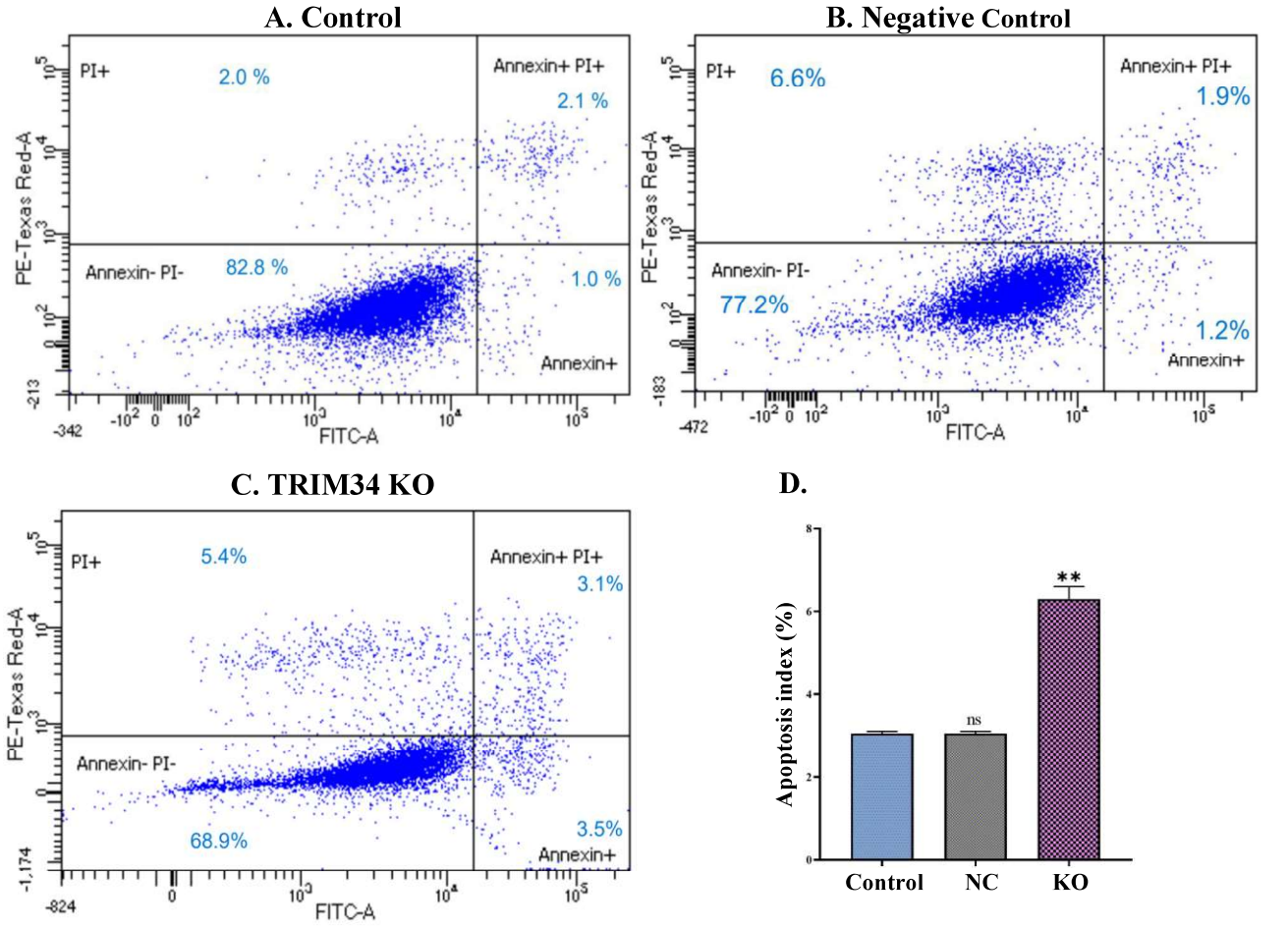

Figure 2.7: Assessment of apoptosis in NCI-H23 cells with *TRIM34* CRISPR/Cas9 Knockout using Annexin V-FITC and PI staining. NCI-H23 cells were stained with Annexin V-FITC and propidium iodide (PI) to assess apoptosis. Representative FACS plot showing the distribution of live cells (Annexin V-FITC negative, PI negative), early apoptotic cells (Annexin V-FITC positive, PI negative), late apoptotic cells (Annexin V-FITC Positive, PI Positive) and necrotic cells (Annexin V-FITC negative, PI Positive). **A.** Control (Untreated) cells, **B.** Negative control group: cells transfected with CRISPR/Cas9 lacking Guide RNA **C.** *TRIM34* CRISPR/Cas9 KO transfected cells. **D.** Apoptosis index (%): Quantification of the percentage of early and late apoptotic in each group, ** stands for $p \leq 0.01$ to indicate statistical significance.

Cell Cycle analysis using FACS.

Cells were subjected to cell cycle analysis using propidium iodide (PI) staining and flow cytometry (FACS). Control group showed a sub-G1 population of 24.9% (Fig. 2.8A&D), while in Negative Control group had 23.85% (Fig. 2.8B&D), and in *TRIM34* CRISPR/Cas9 KO transfection group showed a significantly higher sub-G1 population of 34.15% (Fig. 2.8C&D). This significant increase ($p \leq 0.01$) in the sub-G1 population in the KO group suggests a greater occurrence of apoptosis due to DNA fragmentation compared to the Control group. However, no significant changes were observed in other cell cycle populations (G0/G1, S, and G2/M) between the experimental groups. These results suggest that the knockout of the *TRIM34* gene specifically promoted apoptosis without affecting the distribution of cells in other phases of the cell cycle.

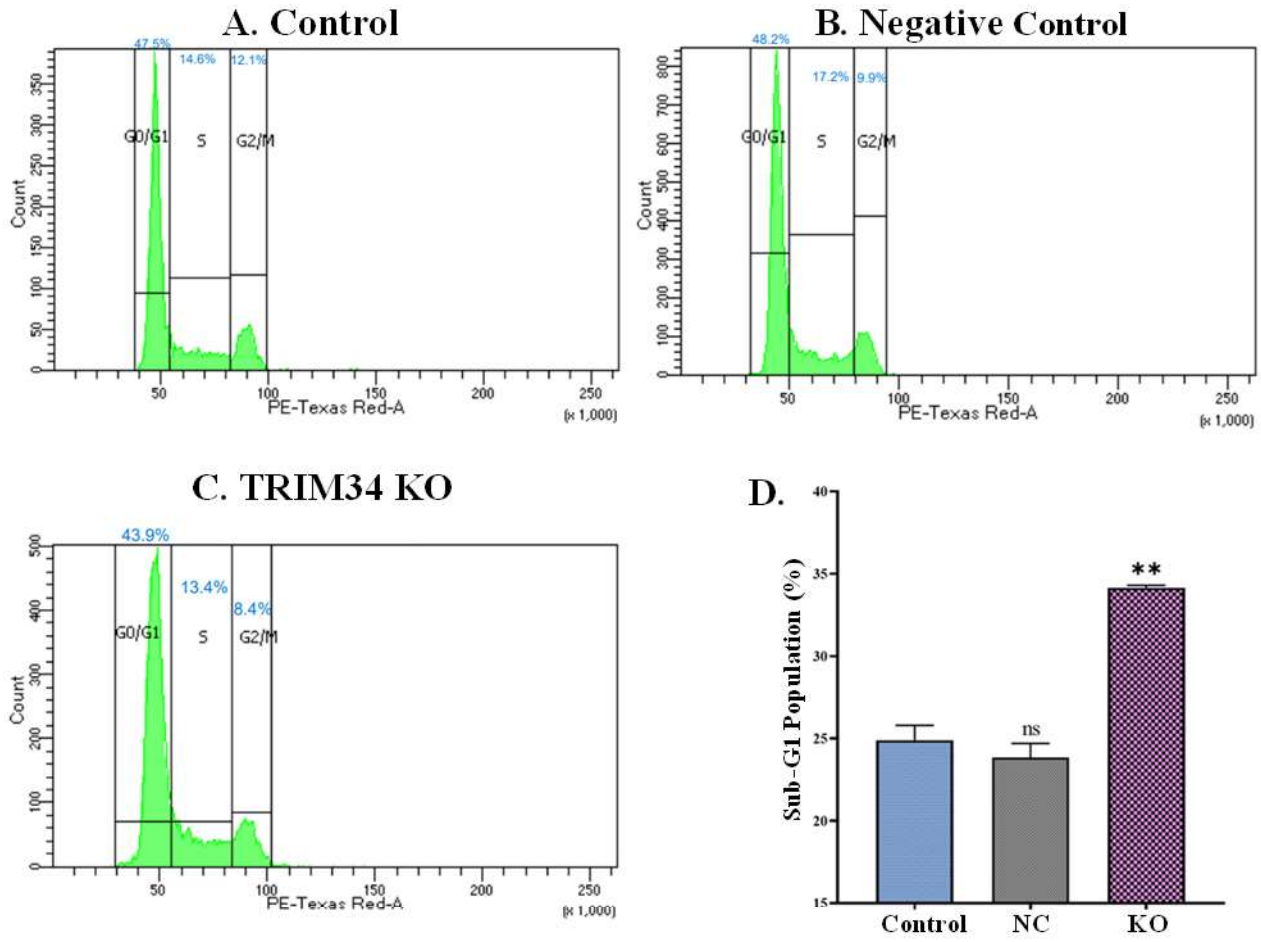

Figure 2.8: Cell cycle analysis of NCI-H23 cells with *TRIM34* CRISPR/Cas9 Knockout using PI staining and FACS. Representative FACS plot showing the distribution of cells in different cell cycle phases, including G0/G1, S, G2/M, and the sub-G1 population representing apoptotic cells with fragmented DNA. **A.** Control (Untreated) Cells, **B.** Negative control group: cells transfected with CRISPR/Cas9 lacking guide RNA **C.** *TRIM34* CRISPR/Cas9 KO transfected cells. **D.** Sub-G1 population (%): Quantification of the percentage of cells in the sub-G1 phase (apoptotic cells) in each group, ** stands for $p \leq 0.01$ to indicate statistical significance.

Identification of top 10 DEG from the entire transcriptomic dataset of *TRIM34* knockout.

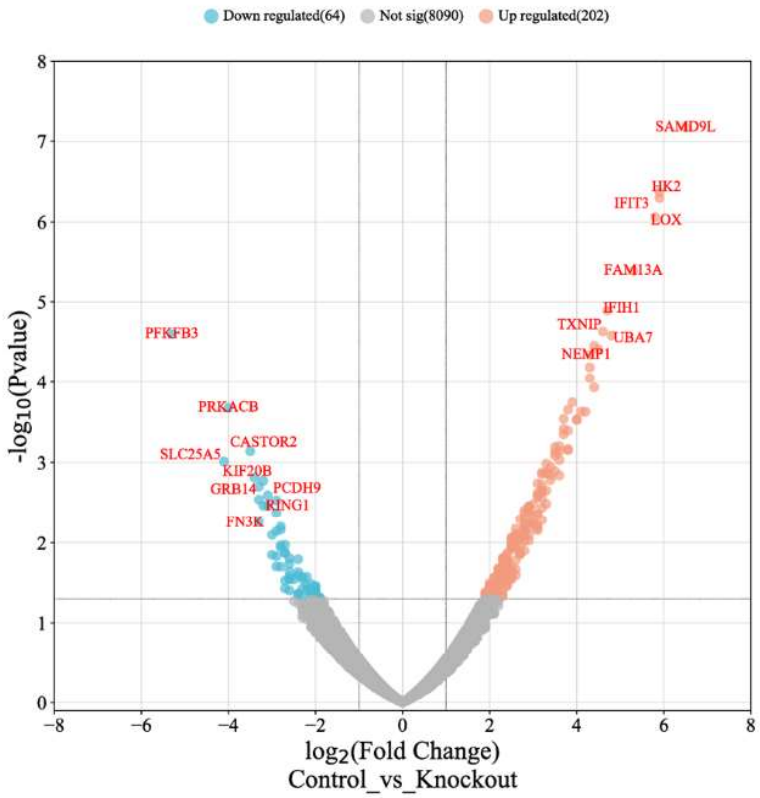

Figure 2.9: Differentially gene expression of *TRIM34* Knockout sample.

Volcano plot depicting differentially expressed genes (DEGs) in *TRIM34* knockout samples compared to control. Genes with a log fold change (log FC) $\geq \pm 2$ and a $p \leq 0.05$ are highlighted, with upregulated genes shown in orange and downregulated genes in blue.

The role of *TRIM34* in regulating gene expression has been investigated through knockout experiments, comparing expression profiles with control sample. Our findings revealed significant alterations in gene expression, with 204 genes upregulated and 69 genes downregulated in *TRIM34* knockout samples compared to the control. The top 10 most upregulated (Table 18) and downregulated (Table 19) genes were selected based on their log FC and *p*-value by using a volcano plot, shedding light on potential molecular mechanisms affected by *TRIM34* knockout. These findings provide insight into potential molecular mechanisms influenced by *TRIM34* knockout in gene expression regulation.

Table 18: Highest upregulated genes in the *TRIM34* Knockout sample.

Gene	Log FC	*p* Value
SAMD9L	6.5	0.000000068
IFIT3	5.9	0.000000503
HK2	5.9	0.000000428
LOX	5.8	0.000000870
FAM13A	5.3	0.000004099
UBA7	4.8	0.000026212
IFIH1	4.7	0.000012816
TXNIP	4.6	0.000023415
NEMP1	4.5	0.000039183
IRF9	4.4	0.000035279

Table 19: Highest downregulated genes in the *TRIM34* Knockout sample.

Gene	Log FC	*p* Value
PFKFB3	-5.3	0.000025
SLC25A5	-4.1	0.000973
PRKACB	-4.0	0.000210
CASTOR2	-3.5	0.000726
KIF20B	-3.4	0.001540
RING1	-3.3	0.002888
GRB14	-3.3	0.001991
FN3K	-3.3	0.005484
PCDH9	-3.2	0.001682
SEPTIN2	-3.2	0.003419

Identifying hub genes from *TRIM34* knockout differentially expressed genes.

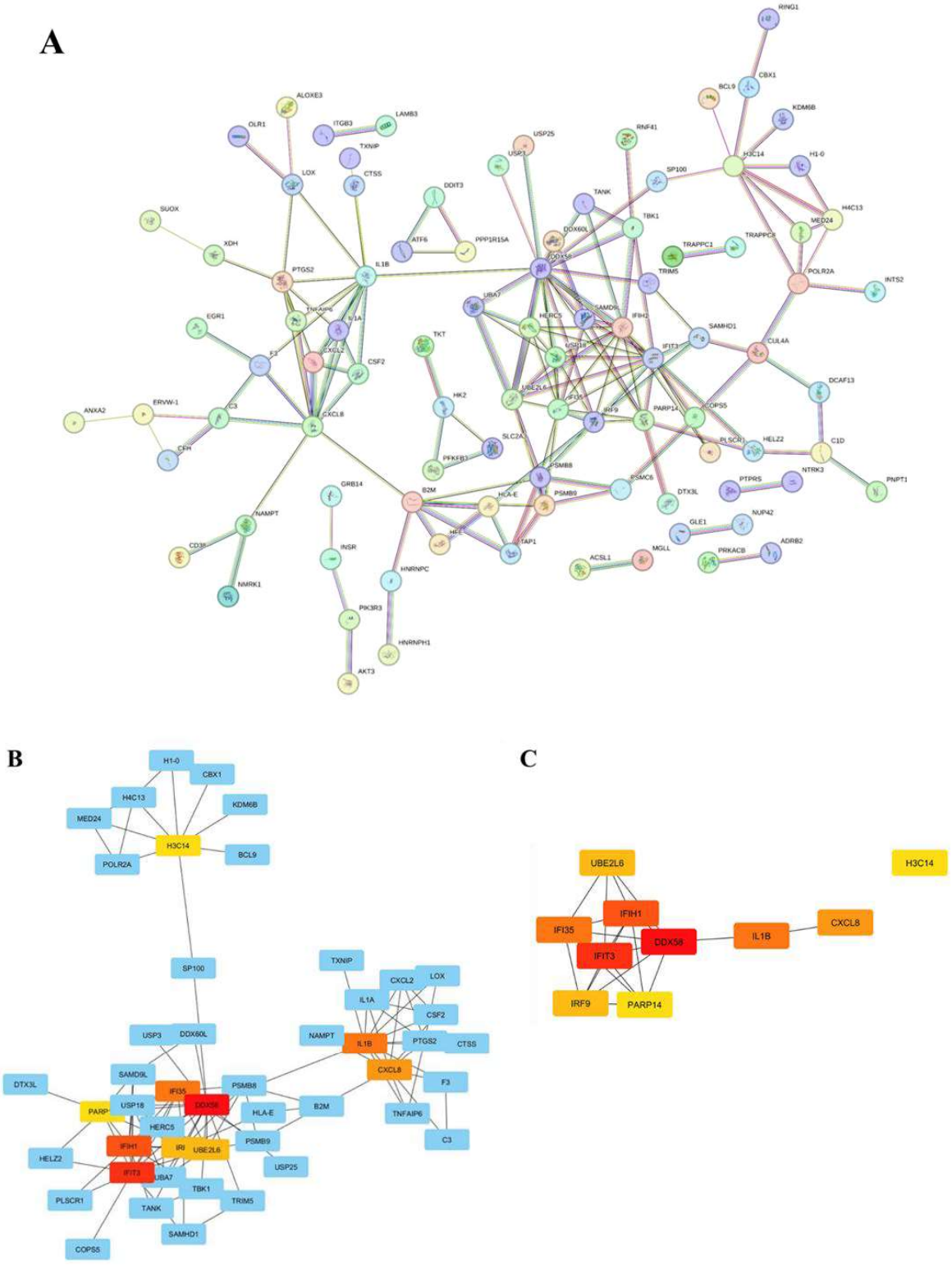

Figure 2.10: The results of the CytoHubba analysis for the 10 hub genes associated with differential expressed genes (A-C) from *TRIM34* knockout samples. Within the CytoHubba network, nodes exhibit a spectrum from red to yellow, reflecting their ranking from the highest to the lowest based on the degree ranking method.

We conducted this experiment intending to discern ubiquitylation genes among the top 10 hub genes. The presented results outline the top 10 differential genes (Table 20) within a network, ranked by the degree ranking method based on their interactions in the String database. *DDX58* holds the highest rank with a score of 18, followed by *IFIT3* with a score of 14 and *IFIH1* with a score of 12. Tied at the fourth position are *IL1B* and *IFI35*, each scoring 11. The subsequent genes in the ranking include *CXCL8* at 6th place with a score of 10, *UBE2L6* and *IRF9* sharing the 7th position with a score of 9 each, and finally, *PARP14* and *H3C14* jointly occupying the 9th position with a score of 8. These scores are indicative of the nodes' centrality and importance in the network, with higher scores suggesting greater connectivity and influence within the biological system under investigation. The initial observation reveals that the top-ranked gene, *DDX58*, with a high score, is linked to ubiquitylation[304,305]. Additionally, the sixth-ranked ubiquitin conjugating enzyme E2 L6 (*UBE2L6*) gene is also associated with ubiquitylation[306,307].

Table 20: Top 10 differential genes in network String interactions ranked by degree ranking method.

Rank	Name	Score
1	*DDX58*	18
2	*IFIT3*	14
3	*IFIH1*	12
4	*IL1B*	11
4	*IFI35*	11
6	*CXCL8*	10
7	*UBE2L6*	9
7	*IRF9*	9
9	*PARP14*	8
9	*H3C14*	8

GO and KEGG enrichment analysis on genes affected by *TRIM34* knockout.

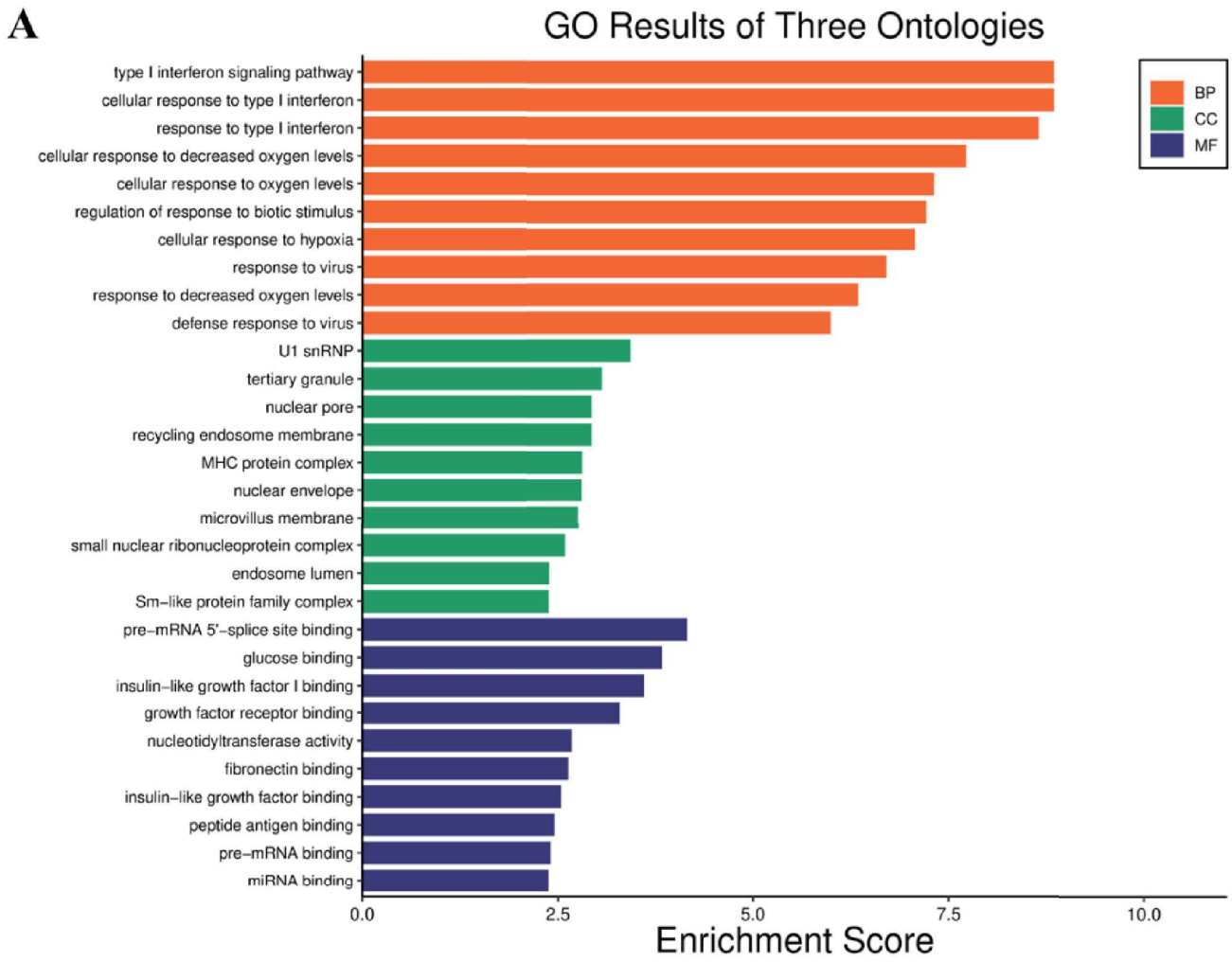

Figure 2.11A: Schematic representation of the Gene Ontology (GO) enrichment analysis workflow. Upregulated genes from *TRIM34* knockout samples in lung adenocarcinoma were subjected to GO term enrichment analysis, categorizing them into distinct functional categories encompassing biological processes (BP), molecular functions (MF), and cellular components (CC). The analysis revealed prominent involvements in key biological pathways and molecular functions, shedding light on the intricate functional landscape of the *TRIM34* gene expression alterations.

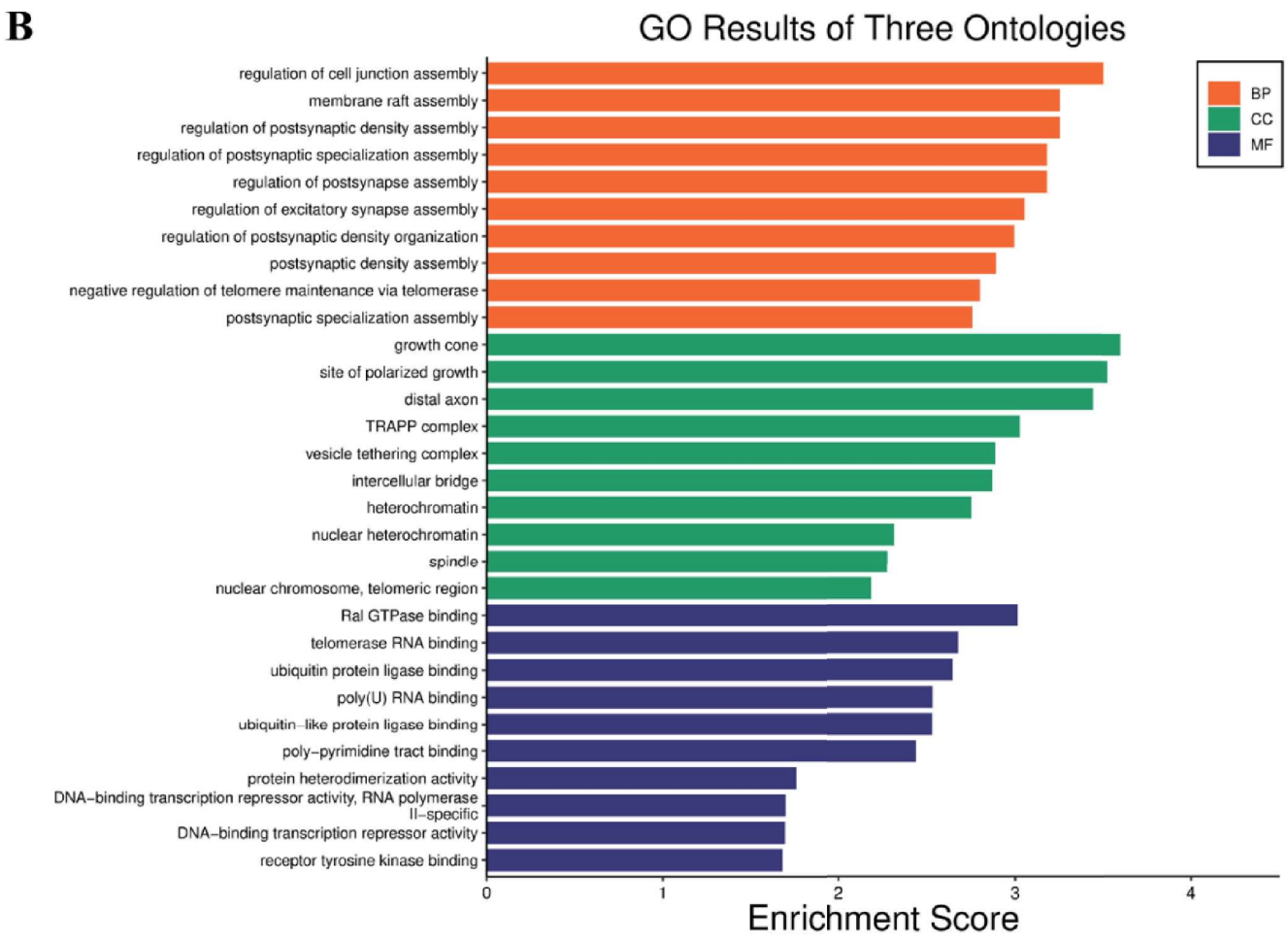

Figure 2.11B: Schematic representation of the Gene Ontology (GO) enrichment analysis workflow. Downregulated genes from *TRIM34* knockout samples in lung adenocarcinoma were subjected to GO term enrichment analysis, categorizing them into distinct functional categories encompassing biological processes (BP), molecular functions (MF), and cellular components (CC). The analysis revealed prominent involvements in key biological pathways and molecular functions, shedding light on the intricate functional landscape of the *TRIM34* gene expression alterations.

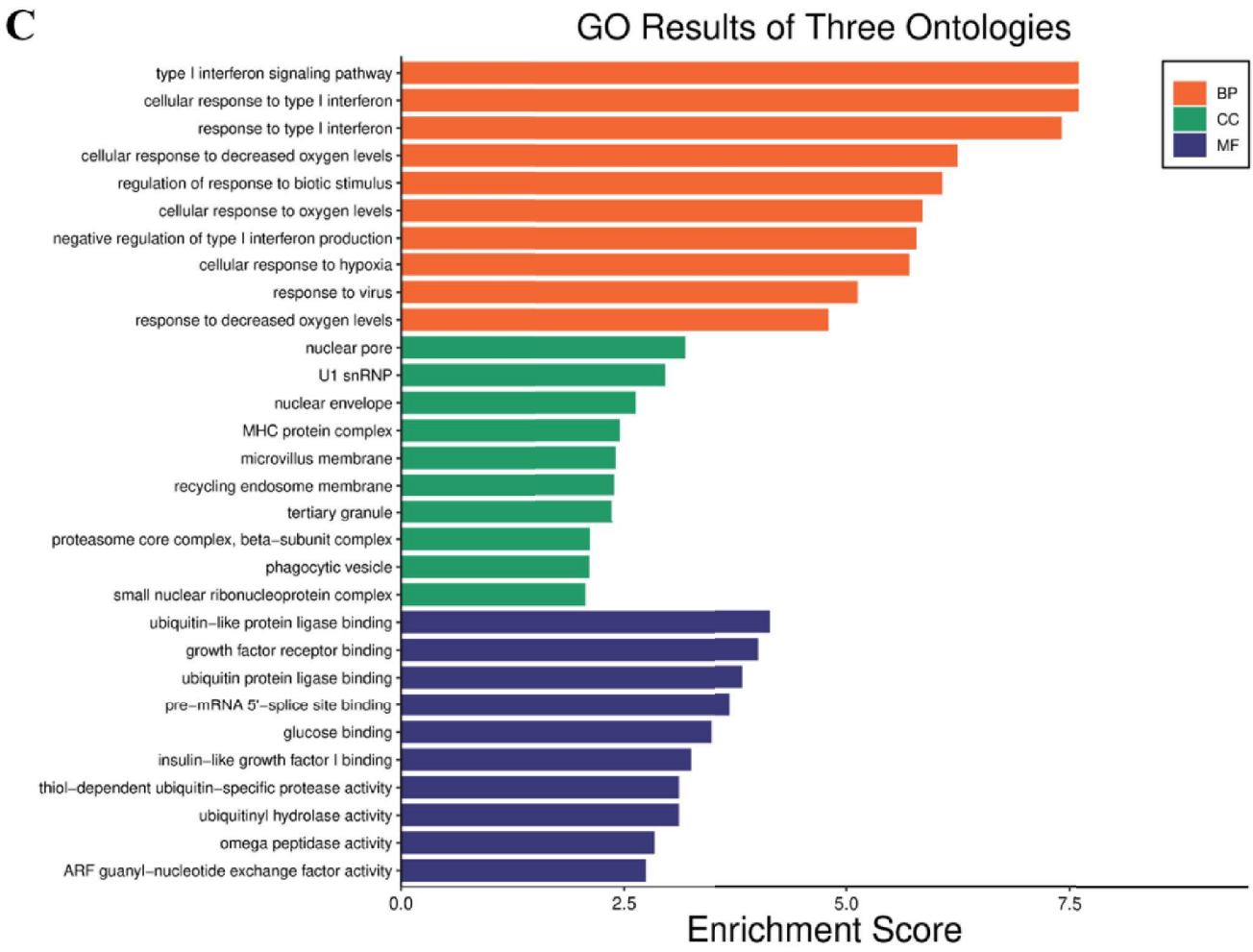

Figure 2.11C: Schematic representation of the Gene Ontology (GO) enrichment analysis workflow. Differential expressed genes from *TRIM34* knockout samples in lung adenocarcinoma were subjected to GO term enrichment analysis, categorizing them into distinct functional categories encompassing biological processes (BP), molecular functions (MF), and cellular components (CC). The analysis revealed prominent involvements in key biological pathways and molecular functions, shedding light on the intricate functional landscape of the *TRIM34* gene expression alterations.

Conducted GO and KEGG enrichment analysis on genes affected by *TRIM34* knockout to identify the pathways, cellular compartments, and molecular functions most significantly impacted. From the upregulated genes (Fig 2.11A), it is evident that several biological processes are affected, including type I interferon signaling pathway, cellular responses to type I interferon, response to type I interferon, cellular response to decreased oxygen levels, cellular response to oxygen levels, regulation of response to biotic stimulus, cellular response to hypoxia, response to viral, response to decreased oxygen levels, and defense responses to viruses was evident. Moreover, cellular component analysis predominantly highlighted constituents encompassing U1 small nuclear ribonucleoprotein particle (U1 snRNP), tertiary granule, nuclear pore, recycling endosome membranes, major histocompatibility complex (MHC) protein complex, nuclear envelope, microvillus membrane, small nuclear ribonucleoprotein complex, endosome lumen, and Sm-like protein family complexes. In the domain

of molecular functions, discernible enrichments were observed for pre-mRNA 5'-splice site binding, glucose binding, insulin-like growth factor I binding, growth factor receptor binding, nucleotidyltransferase activity, fibronectin binding, insulin-like growth factor binding, peptide antigen binding, pre-mRNA binding, and miRNA binding.

Delving into the networked biological process terms in downregulated genes (Fig 2.11B), a prominent thematic underpinning encompassed the regulation of cell junction assembly, membrane raft assembly, regulation of postsynaptic density assembly, regulation of postsynaptic specialization assembly, regulation of postsynapse assembly, regulation of excitatory synapse assembly, regulation of postsynaptic density organization, postsynaptic density assembly, negative regulation of telomere maintenance via telomerase, postsynaptic specialization assembly. The ensuing cellular component analysis accentuated entities intrinsic to the growth cone, site of polarized growth, distal axon, TRAPP complex, vesicle tethering complex, intercellular bridge, heterochromatin, nuclear heterochromatin, spindle, nuclear chromosome, and telomeric region. Notably, the enrichment of molecular function terms predominantly included associations with Ral GTPase binding, telomerase RNA binding, ubiquitin protein ligase binding, poly(U) RNA binding, ubiquitin-like protein ligase binding, poly-pyrimidine tract binding, protein heterodimerization activity, DNA-binding transcription repressor activity, RNA polymerase II-specific, DNA-binding transcription repressor activity, receptor tyrosine kinase binding. These intricate findings collectively illuminate the nuanced functional repertoire of the examined differentially expressed genes consequent to *TRIM34* knockout within the intricate context of lung adenocarcinoma, thereby shedding light on their pivotal involvements across multifarious biological, molecular, and cellular dimensions.

The present investigation pursued the discernment of distinctive biological attributes intrinsic to differentially expressed genes (Fig 2.11C). The resultant analysis of networked biological process terms highlighted a prevailing involvement in pivotal processes, notably the type I interferon signaling pathway, cellular response to type I interferon, response to type I interferon, cellular response to decreased oxygen levels, regulation of responses to biotic stimulus, cellular response to oxygen level, and negative regulation of type I interferon production, cellular response to hypoxia, response to virus, and response to decreased oxygen levels. Concomitantly, the analysis of cellular components predominantly spotlighted constituents encompassing the nuclear pore complex, U1 snRNP, the nuclear envelope, MHC protein complex, microvillus membrane, recycling endosome membrane, tertiary granule, proteasome core complexes, beta-subunit complex, phagocytic vesicle, and small nuclear ribonucleoprotein complex. Notably, molecular function terms exhibited prominent enrichments, including associations with ubiquitin-like protein ligase binding, growth factor receptor binding, ubiquitin protein ligase binding, pre-mRNA 5'-splice site binding, glucose binding, insulin-like growth factor I binding, thiol-dependent ubiquitin-specific proteases activity, ubiquitinyl

hydrolases, and omega peptidases, as well as ARF guanyl-nucleotide exchange factor activity. These intricate findings collectively illuminate the multifaceted functional list of the examined differentially expressed genes consequent to *TRIM34* knockout within the intricate context of lung adenocarcinoma, thereby unraveling their pivotal involvements across diverse biological, molecular, and cellular dimensions.

Collectively, notable changes were noted in biological processes, including alteration in type I interferon signaling, the initiation of a defensive response against viruses, a reduction in oxygen levels leading to hypoxic conditions, and primarily, a diminished molecular function related to ubiquitylation in *TRIM34* deficient condition. These findings suggest that *TRIM34* mainly plays a crucial role in regulating ubiquitylation, oxygen levels, and interferon signaling in lung cancer.

Enrichment analysis of molecular functions on genes affected by *TRIM34* deficient condition.

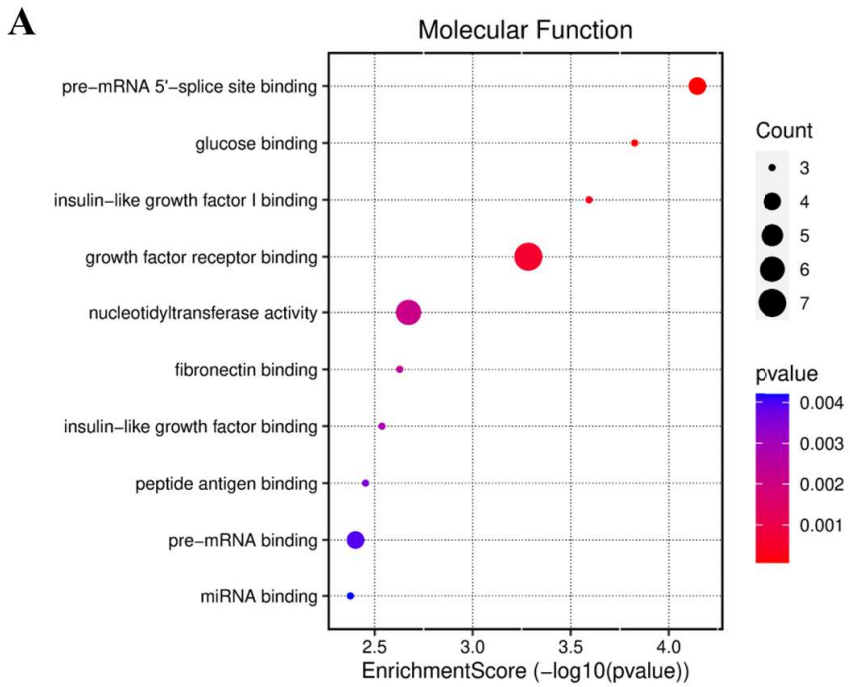

Figure 2.12A: Utilizing Gene Ontology (GO) and Kyoto Encyclopedia of Genes and Genomes (KEGG) pathway analysis, Enrichment analysis of molecular functions was performed on the upregulated genes within the TRIM knockout sample. The bubble plot visually presents the top 10 enriched pathways, ranked by their False Discovery Rate (FDR) *p*-values. Along the Y-axis, pathways are labeled, while the X-axis displays the Enrichment Score (-log10 (*p*-value)). Bubbles in the plot vary in size based on the number of genes related to the enriched pathway, and their color corresponds to the corrected *p*-value of the specific enriched pathway.

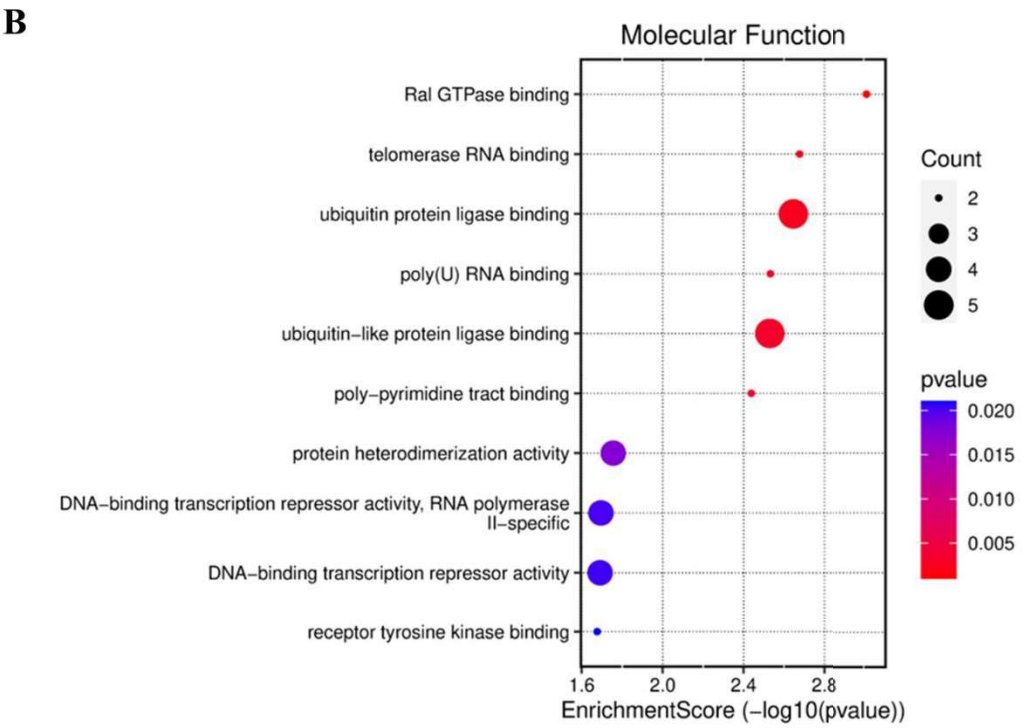

Figure 2.12B: Utilizing Gene Ontology (GO) and Kyoto Encyclopedia of Genes and Genomes (KEGG) pathway analysis, Enrichment analysis of molecular functions was performed on the downregulated genes within the TRIM knockout sample. The bubble plot visually presents the top 10 enriched pathways, ranked by their False Discovery Rate (FDR) *p*-values. Along the Y-axis, pathways are labeled, while the X-axis displays the Enrichment Score (-log10 (*p*-value)). Bubbles in the plot vary in size based on the number of genes related to the enriched pathway, and their color corresponds to the corrected *p*-value of the specific enriched pathway.

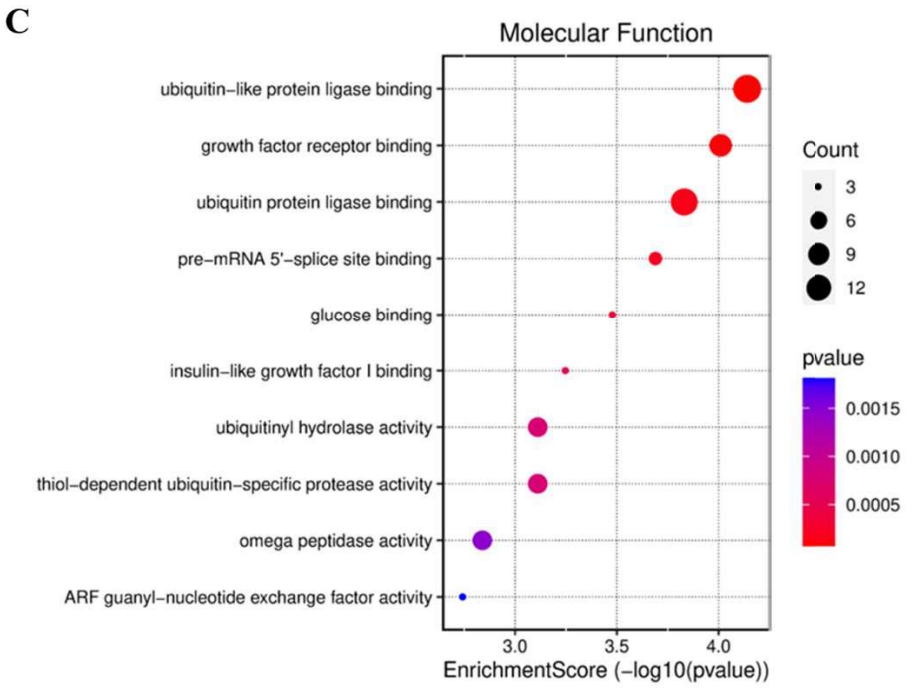

Figure 2.12C: Utilizing Gene Ontology (GO) and Kyoto Encyclopedia of Genes and Genomes (KEGG) pathway analysis, Enrichment analysis of molecular functions was performed on the differential genes within the TRIM knockout sample. The bubble plot visually presents the top 10 enriched pathways, ranked by their False Discovery Rate (FDR) *p*-values. Along the Y-axis, pathways are labeled, while the X-axis displays the Enrichment Score (-log10 (*p*-value)). Bubbles in the plot vary in size based on the number of genes related to the enriched pathway, and their color corresponds to the corrected *p*-value of the specific enriched pathway.

Based on the results of the molecular functions mentioned above, we proceeded to identify the more significant functions by examining their enrichment scores. To achieve this, we conducted additional enrichment analysis. It is noteworthy that growth factor receptor binding exhibits a significant upregulation (Fig. 2.12A) compared to other molecular functions, whereas ubiquitin-related binding activity experiences a significant downregulated (Fig. 2.12B). The analysis of enrichment indicates that, within the top 10 pathways, four are linked to ubiquitylation in differential genes (Fig. 2.12C). This implies that the TRIM34 has a considerable impact on the ubiquitylation process in NSCLC.

Exploring genes and their corresponding molecular functions using a Circos plot method

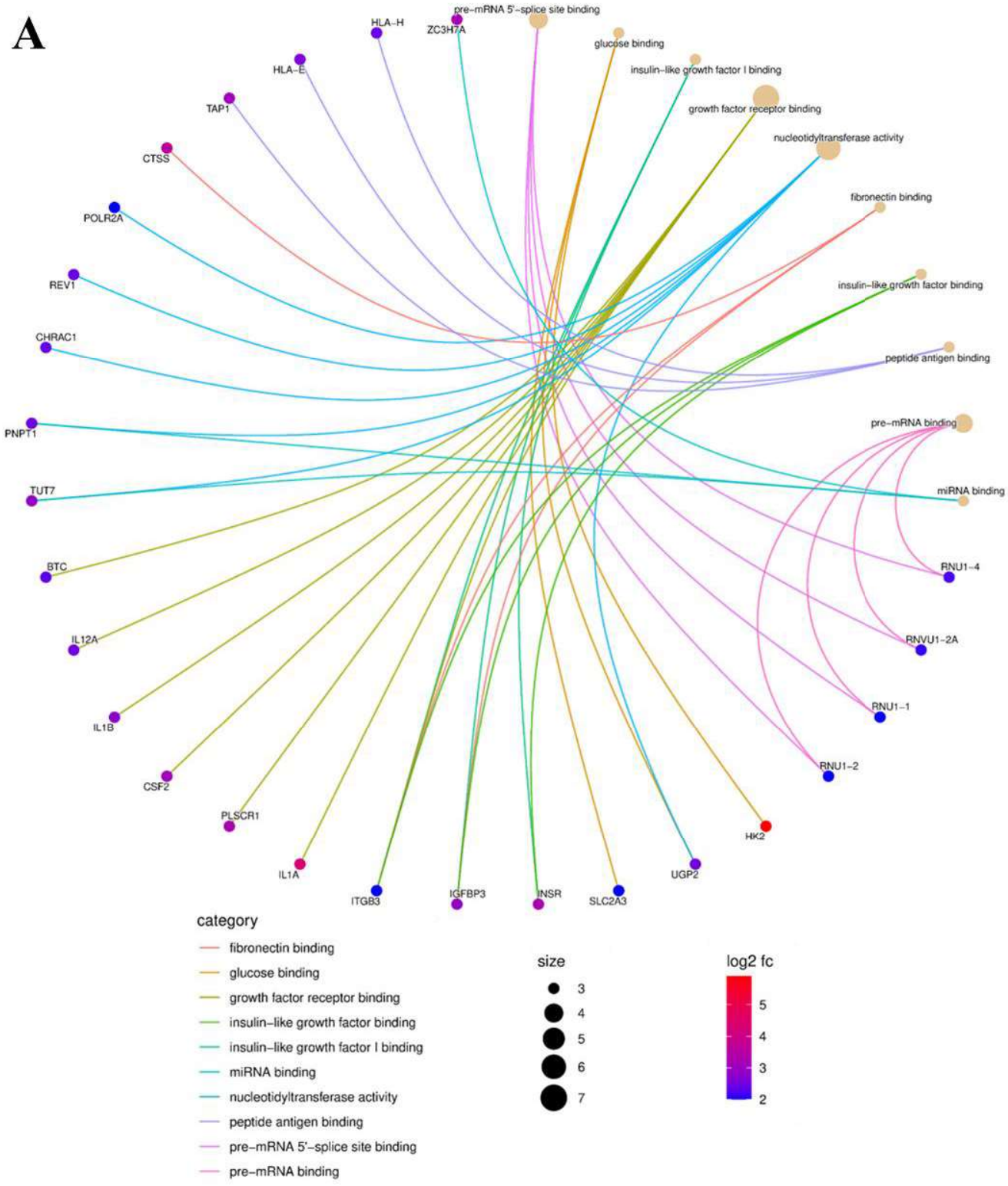

Figure 2.13A: Investigating genes and their associated molecular functions utilizing the Circos plot of upregulated genes in *TRIM34* knockout.

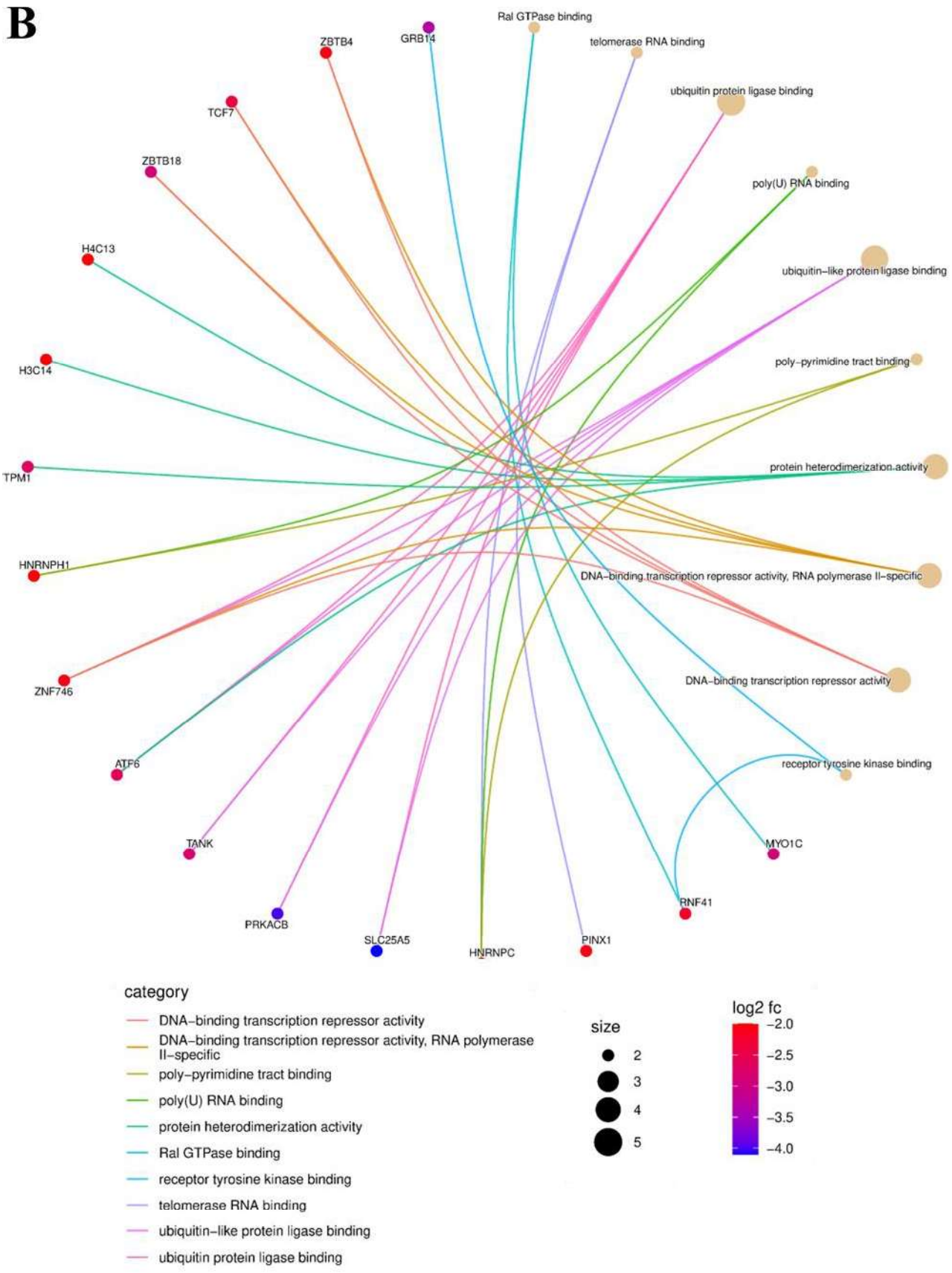

Figure 2.13B: Investigating genes and their associated molecular functions utilizing the Circos plot of downregulated genes in *TRIM34* knockout.

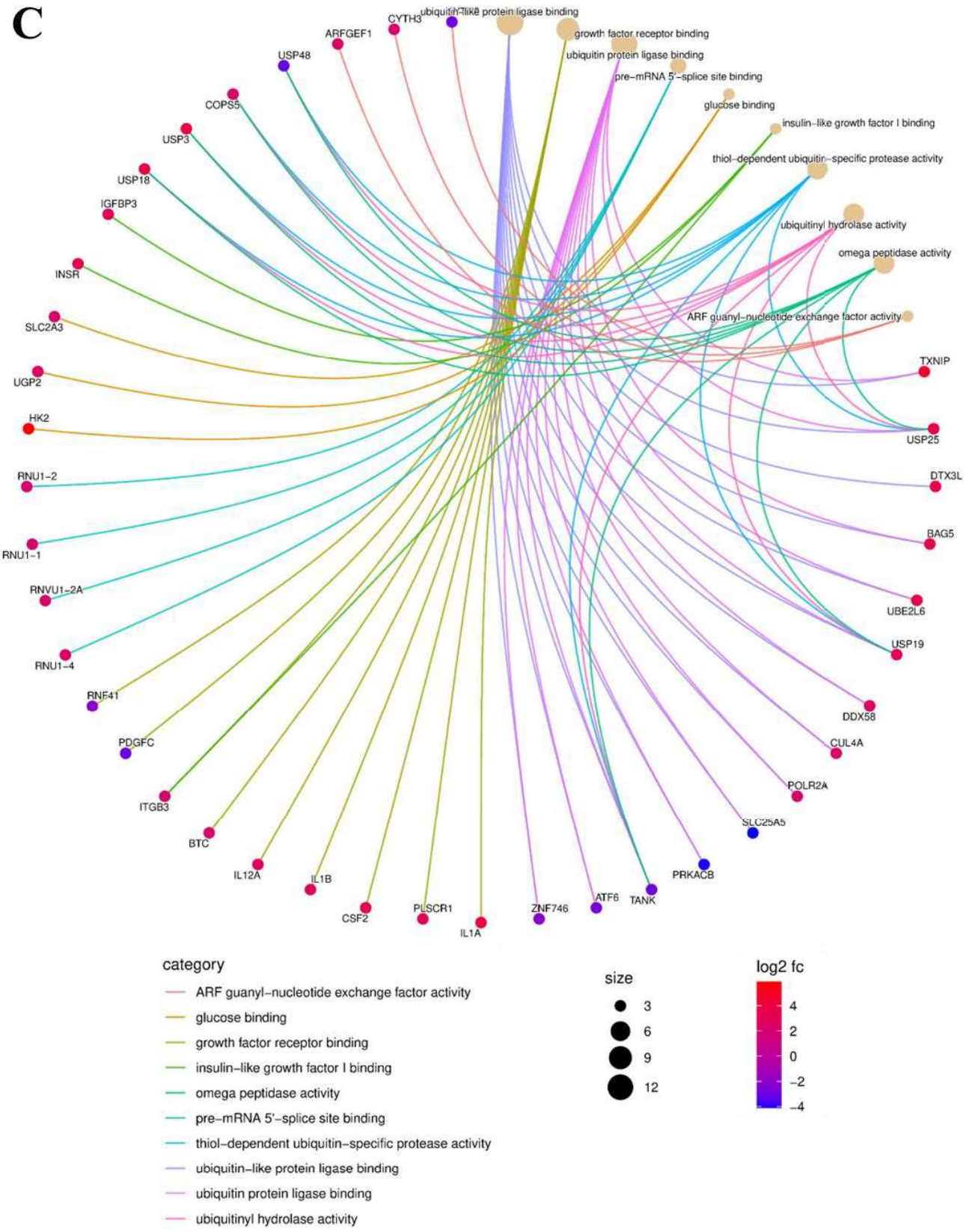

Figure 2.13C: Investigating genes and their associated molecular functions utilizing the Circos plot of differential genes in *TRIM34* knockout.

Circos plot, a specialized data visualization tool, indicates that the analysis employs a comprehensive and visually informative approach to present the relationships between genes and their respective molecular functions. This approach allows for a more in-depth understanding of the molecular landscape affected by the *TRIM34* knockout, enhancing the interpretation of the experimental results.

Furthermore, we extended our analysis to identify molecular functions along with their respective genes. Specifically, we focused on the top 10 molecular functions and their corresponding genes derived from the Differentially expressed genes (DEGs) in the *TRIM34* knockout condition. This information was visualized and presented through a Circos plot, allowing for a comprehensive and visually informative representation of the molecular functions associated with the affected genes. We did not discover any genes related to the ubiquitylation pathway in the top 10 list, as reflected in Fig. 2.13A. However, upon examining all significantly upregulated genes (log FC $\geq$ +2, $p \leq 0.05$) outside the Circos plot, we identified several relevant genes by GO (Table 21). On the other hand, the Circos plot enabled the identification of the most downregulated genes associated with the ubiquitin pathway, including SLC25A5, PRKACB, TANK, ATF6, and ZNF746 (Fig. 2.13B&C). Additionally, other genes such as USP48 and RING1 were discovered among all significantly downregulated genes (log FC $\geq$ -2, $p \leq 0.05$) outside the Circos plot by GO (Table 22).

Table 21: Upregulated ubiquitin pathway genes identified by GO analysis in the *TRIM34* knockout sample.

ID	Description	Genes
GO:0044389	Ubiquitin-like protein ligase binding	*TXNIP, USP25, DTX3L, BAG5, UBE2L6, USP19, DDX58, CUL4A, POLR2A*
GO:0004843	Thiol-dependent ubiquitin-specific protease activity	*USP18, USP3, USP25, USP19, COPS5*
GO:0101005	Ubiquitinyl hydrolase activity	*USP18, USP3, USP25, USP19, COPS5*
GO:0019787	Ubiquitin-like protein transferase activity	*UBA7, DTX3L, FBXW11, UBE2L6, HERC5, TRIM5, KIAA1586, CUL4A, RC3H2, UBR4, TRIM38*
GO:0031625	Ubiquitin protein ligase binding	*TXNIP, USP25, BAG5, UBE2L6, USP19, DDX58, CUL4A, POLR2A*

Table 22: Downregulated ubiquitin pathway genes identified by GO analysis in the *TRIM34* knockout sample.

ID	Description	Genes
GO:0031625	Ubiquitin protein ligase binding	*SLC25A5, PRKACB, TANK, ATF6, ZNF746*
GO:0044389	Ubiquitin-like protein ligase binding	*SLC25A5, PRKACB, TANK, ATF6, ZNF746*
GO:0004843	Thiol-dependent ubiquitin-specific protease activity	*USP48, TANK*
GO:0101005	Ubiquitinyl hydrolase activity	*USP48, TANK*
GO:0055106	Ubiquitin-protein transferase regulator activity	*RING1*

DISCUSSION

Lung adenocarcinoma, a prevalent subtype of non-small cell lung cancer (NSCLC), remains a significant global health challenge due to its aggressive nature and resistance to conventional therapies[67,223,224]. Novel therapeutic strategies are urgently needed to target the intricate molecular pathways underpinning its pathogenesis. Ubiquitination, a post-translational modification characterized by the covalent bonding of ubiquitin molecules to specific proteins, serves a diverse function in cellular processes, including protein degradation, DNA repair, and signal transduction. Dysregulation of ubiquitination is implicated in numerous diseases including cancer[293,308,309]. The precision required for mammalian development involves the accurate spatial and temporal positioning of millions of molecules, regulating their functions to coordinate crucial aspects of cell cycle progression, apoptosis, migration, and differentiation in developing embryos. Ubiquitin and its associated enzymes serve as cellular guardians, ensuring precise control over key molecules during these processes. Disruptions in this precision contribute to embryological disorders[124,310] and cancer[293,294]. E3 ubiquitin ligases are crucial in early mammalian development, linked to human diseases. Manipulating ubiquitin regulation holds therapeutic promise via molecular glues and PROTACs[311].

TRIM proteins, function as E3 ubiquitin ligases, catalyzing the transfer of ubiquitin moieties to substrates. TRIM34 has garnered attention for its diverse roles, studies show TRIM34's regulatory

functions in interferon response, and its antiviral role against HIV-1[270,299,312]. It also has a protective role in colon cancer by inducing apoptosis[218]. Additionally, TRIM34 interacts with ZBP1, promoting K63-linked polyubiquitination and triggering programmed cell death and inflammation, offering protection against influenza A virus-related death[300]. Observing these findings, we aimed to identify sensitive ubiquitination pathway genes under TRIM34 knockout conditions.

The intricate molecular landscape underlying NSCLC progression is elucidated through various molecular interactions and regulatory pathways. The changes observed in ubiquitylation-associated genes due to the deficiency of TRIM34 may play a role in the pathogenesis of lung cancer. The alterations in these genes could contribute to the development or progression of lung cancer, indicating a potential association between TRIM34 deficiency and the molecular mechanisms involved in the disease.

In the *TRIM34* knockout condition, upregulation was observed in ubiquitination-associated genes, including *TXNIP, USP25, DTX3L, BAG5, UBE2L6, USP19, DDX58, CUL4A, POLR2A, USP18, USP3, COPS5, UBA7, FBXW11, HERC5, TRIM5, KIAA1586, RC3H2, UBR4, and TRIM38* (Table 21). Liang *et al.* (2021) have shown the involvement of TXNIP in lung cancer, they have seen that CircDCUN1D4 engages in base complementation to directly interact with TXNIP mRNA, forming the circDCUN1D4/HuR/TXNIP RNA-protein ternary complex, thereby inhibiting lung cancer cell metastasis and glycolysis[313]. Li *et al.* (2015) observed that under hypoxic conditions, TXNIP expression is heightened in NSCLC, signifying a potential prognostic indicator[314]. Further Kim *et al.* (2022) have shown that the lipid molecule 1-palmitoyl-2-linoleoyl-3-acetyl-rac-glycerol (PLAG) impedes tumor progression by instigating the degradation of adenosine 2B receptors (A2BRs) in tumors, promoting TXNIP-mediated A2BR internalization and degradation, consequently hindering lung tumor growth[315].

High-risk human papillomavirus 16 (HPV16) infection correlates with lung cancer, and the associated E6/E7 proteins modulate GLUT1 expression through the PTEN-TXNIP-HIF-1α axis, impacting glucose uptake[316]. In lung cancer, hypoxia reduces Itchy E3 ubiquitin-protein ligase (ITCH) expression, promoting migration, invasion, ROS production, inflammation, and apoptosis in LC cells; ITCH overexpression counteracts these effects by degrading TXNIP [317]. Cyclophilin A (cypA) overexpression in NSCLC, especially under hypoxia, correlates with poor survival. CypA acts as an oncogene by binding to and degrading TXNIP, promoting cell growth and inhibiting cell death [318]. Cheng *et al.* (2022) have shown that LHFPL3-AS2, reduced in NSCLC, hinders invasion by interacting with SFPQ, suppressing TXNIP transcription [319]. Ceramide induces apoptosis in lung adenocarcinoma cells by modulating the Txnip/Trx1 complex [320]. Sodium butyrate induces TRAF6-dependent TXNIP expression in NSCLC, impacting migration and proliferation[321]. MAGI2-AS3

downregulation in NSCLC promotes cell proliferation and invasion; overexpression has the opposite effect by inhibiting miR-629-5p and suppressing TXNIP expression [322]. Becker *et al.* (2018) seen the impact of influenza A virus (IAV) treatment on lung cancer cell lines was investigated, revealing the up-regulation of Ubiquitin Conjugating Enzyme E2 L6 (UBE2L6). This up-regulation was associated with enhanced modification of the viral NS1 protein by the immune-related protein ISG15[323]. Liao *et al.* (2020) have observed that Ubiquitin specific protease 3 (USP3) is significantly upregulated in NSCLC tumor tissues, correlating with advanced pathology stage and lower survival rates. RNA Binding Motif 4 (RBM4) is identified as a target for USP3, and rescue experiments confirm RBM4's role in mediating NSCLC progression regulated by USP3[324]. Liu *et al.* (2021) observed that Ubiquitin specific peptidase 18 (USP18), known as the IFN-stimulated gene 15 (ISG15), promotes tumorigenesis by modulating adipose triglyceride lipase (ATGL) and uncoupling protein 1 (UCP1), affecting fatty acid metabolism.

Lung cancers with increased USP18, ATGL, and UCP1 expression have poor survival[325]. Reducing USP18 in lung cancer cells significantly inhibits growth, migration, invasion, and metastasis. The study identifies 14-3-3ζ as a key protein regulated by USP18, impacting lung cancer metastasis[326]. Li *et al.* (2014) have shown that miR-200c overexpression inhibits NSCLC cell migration, invasion, and EMT by targeting Ubiquitin Specific Peptidase 25 (USP25). Clinical analysis shows a negative correlation between miR-200c and NSCLC progression, while USP25 expression is elevated in NSCLC patients, correlating with disease stage and lymph node metastasis[327]. P53, a critical DNA damage response regulator, interacts with Poly ADP-ribose polymerase 1 (PARP1) at damaged DNA sites. Deltex-3-like (DTX3L), recruited to PARP1-PARylated sites, polyubiquitylates p53, leading to its proteasomal degradation. DTX3L knockout enhances and prolongs p53 retention at these sites. Inhibiting DTX3L could potentially increase p53 abundance and activity, improving the efficacy of certain DNA-damaging agents[328]. Li *et al.* (2010) have shown that BAG-5 expression in cancer tissues was significantly low, signifying a protective factor for lung adenocarcinoma[329]. Yu *et al.* (2022) conducted a study exploring the connection between ischemic heart failure (HF) and cancer, which has been on the rise. They identified DDX58 as a key immune-related gene associated with ischemic HF and found it highly expressed in many cancer types. High DDX58 expression negatively impacted prognosis in various tumors and correlated with immune cell infiltration and immune checkpoint gene expression [330].

In NSCLC, overexpressed Cullin-4A (Cul4A) correlates with poor prognosis and diminished ANXA10. Cul4A suppression inhibits cancer cell invasion by upregulating ANXA10 through direct interaction and ubiquitination, influencing lung cancer metastasis [331]. Silencing CUL4A impedes tumor growth by modulating EGFR and AKT activation, with potential therapeutic targeting of EGFR in lung cancer [332]. In lung cancer cells, Cul4A knockdown induces G0/G1 cell cycle arrest, reduces

proliferation, and enhances sensitivity to gemcitabine chemotherapy, associated with increased p21, TIEG1, and TGFBI expression. In xenografts, Cul4A suppression reduces tumor growth and enhances gemcitabine sensitivity [333]. Elevated CUL4A induces ZEB1, fostering epithelial-mesenchymal transition (EMT) and promoting lung adenocarcinoma metastasis to the bone [334]. Mao *et al.* (2020) have found that BCAR1 knockout inhibits lung cancer cell growth and colony formation; High POLR2A expression, correlated with BCAR1, predicts poor prognosis in lung cancer cases [335]. COP9 signalosome subunit 5 (COPS5) is identified as a deubiquitinating enzyme for the transcription factor SNAIL, crucial in cancer metastasis. COPS5 downregulation reduces SNAIL expression, inhibiting lung cancer cell metastasis in vitro and in vivo. COPS5 binds to SNAIL, stabilizing its expression through deubiquitylation [336].

Increased Jab1/COPS5 correlated with non-responsiveness to chemotherapy in lung cancer[337]. MiR-182 is significantly upregulated in NSCLC, inversely correlated with FBXW7 and FBXW11. Its overexpression promotes cell growth, colony formation, and cell cycle progression while inhibiting apoptosis in NSCLC cells. Downregulating miR-182 has the opposite effect [338]. Wrage *et al.* (2015) have seen hypermethylation of the HERC5 promoter in NSCLC emerge as a prognostic factor for poor survival in lung adenocarcinoma[339]. Tripartite motif protein 38 (TRIM38) is downregulated in NSCLC. Overexpression of TRIM38 inhibits tumor nodules, epithelial-to-mesenchymal transition (EMT), migration, invasion, and proliferation in NSCLC [340].

In the *TRIM34* knockout condition, downregulation was observed in ubiquitination-associated genes, including SLC25A5, PRKACB, ATF6, ZNF746, USP48, TANK, and RING1 (Table 22). CHEN *et al.* (2013) have found that PRKACB is downregulated in NSCLC but increasing PRKACB levels inhibits cell proliferation, colony formation, and invasion while promoting apoptosis [341]. Inhibiting ZNF746 in NSCLC cells reduces invasion and epithelial-mesenchymal transition (EMT). KIM *et al.* (2014) have shown that ZNF746 inhibition decreases the expression of matrix metalloproteinases (MMPs) and key factors associated with malignancy [342]. Upregulation of miR-489-3p inhibits NSCLC cell proliferation, migration, and EMT. Moreover, miR-489-3p deactivates the Wnt/β-catenin pathway, regulating USP48 to prevent β-catenin ubiquitination [343]. RING1 expression is found to be significantly increased in lung cancer which correlates with advanced TNM stage, proliferation, and poor prognosis. While RING1 knockdown inhibits lung cancer cell growth through G1/S cell cycle arrest in NSCLC[344].

In TRIM34 deficient condition, a noteworthy phenomenon is evident, wherein certain genes display an increase in expression. Among these, several genes previously recognized for upregulation in lung cancer, such as TXNIP, UBE2L6, USP3, USP18, USP25, DTX3L, DDX58, CUL4A, POLR2A, and COPS5, consistently show elevated levels. Interestingly, this includes genes like BAG5, FBXW11,

HERC5, and TRIM38, typically downregulated in lung cancer but unexpectedly upregulated in the absence of TRIM34.

Conversely, when TRIM34 is deficient, specific genes undergo a reduction in expression. Noteworthy among these are genes like ZNF746, USP48, and RING1, previously identified as upregulated in lung cancer. Intriguingly, the gene PRKACB, typically downregulated in lung cancer, experiences even further downregulation in the absence of TRIM34. These findings unveil a complex interplay of gene expression patterns, suggesting potential regulatory roles for TRIM34 in influencing alterations in gene expression associated with lung cancer.

Further exploration is necessary to clarify the underlying molecular mechanisms and functional implications of these observed genetic responses. Apoptosis, or programmed cell death, plays a crucial role in maintaining tissue homeostasis by eliminating damaged or potentially harmful cells[1]. The experimental results presented here provide compelling evidence that *TRIM34* knockout triggers apoptotic cell death in lung adenocarcinoma cells. The use of FACS and live-dead assays allowed for the quantification of apoptotic and viable cells, respectively. The significant increase in apoptotic cell death (Fig. 2.7) observed upon *TRIM34* knockout suggests a regulatory role for *TRIM34* in apoptosis modulation. The findings presented in our experiments support the assertion that the elimination of *TRIM34* induces apoptotic cell death in lung adenocarcinoma cells. Although these findings offer valuable insights into the involvement of *TRIM34* in regulating apoptosis, it is crucial to conduct further investigations to elucidate the underlying molecular mechanisms of this phenomenon. The identification of specific pathways and interactions through which *TRIM34* influences apoptosis regulation will enhance our comprehensive understanding of its functional implications in lung adenocarcinoma. Consequently, additional studies are necessary to unravel the intricacies of *TRIM34*-mediated apoptotic modulation, laying the groundwork for potential therapeutic interventions and comprehension of its influence on cellular processes within the context of cancer.

In the context of lung adenocarcinoma, our study explores the intricate relationship between TRIM34, a known E3 ubiquitin ligase, and ubiquitylation-associated genes. Through a comprehensive analysis of molecular interactions and regulatory pathways, we identify alterations in gene expression patterns upon TRIM34 knockout. Interestingly, both upregulation and downregulation of specific genes associated with lung cancer are observed, suggesting a complex regulatory role for TRIM34. Additionally, our findings indicate that TRIM34 knockout induces apoptotic cell death in lung adenocarcinoma cells, emphasizing its potential as a therapeutic target.